Heavy Quark Production In Heavy Ion Colliders

R. Vogt

Nuclear Science Division, Lawrence Berkeley National Laboratory, Berkeley, CA 94720, USA

and

Physics Department, University of California, Davis, CA 95616, USA

Outline

- Updating NLO pp Production Cross Sections
- Effects of Shadowing and p_T Broadening in pA and AA
- Implications for Quarkonium
- Some Comments on the K Factor

Why Update the pp Baseline?

Newer parton densities available now than when the Hard Probes Collaboration was formed: MRST, CTEQ5, GRV 98

These revised parton densities do not exhibit the same features at low x as those used previously (MRS D-' and GRV)

Main difference is the steeper rise as $x \to 0$ of the old densities, leading to huge cross sections at high energies, $\sigma_{c\overline{c}}^{\rm tot} = 17$ mb at 5.5 TeV

The Partonic Cross Sections

$Q\overline{Q}$ production at LO by $q\overline{q}$ annihilation and gg fusion, at NLO, qg and $\overline{q}g$ make a small contribution

Partonic cross sections expressed in terms of dimensionless scaling functions, $f_{ij}^{(k,l)}(\eta = \hat{s}/4m_Q^2 - 1)$,

$$\hat{\sigma}_{ij}(\hat{s}, m_Q^2, \mu^2) = \frac{\alpha_s^2(\mu)}{m^2} \sum_{k=0}^{\infty} \; (4\pi\alpha_s(\mu))^k \sum_{l=0}^{k} \; f_{ij}^{(k,l)}(\eta) \; \ln^l \left(\frac{\mu^2}{m_Q^2}\right)$$

LO: $k = 0$, $l = 0$; NLO: $k = 1$, $l = 0, 1$; NNLO: $k = 2$, $l = 0, 1, 2...$

At LO, $\mu = \mu_F$, the factorization scale in the parton densities

Beyond LO, the renormalization scale μ_R also enters

These scales are normally set equal to each other $\mu = \mu_F = \mu_R$ since they are not separated in the evaluations of the parton densities

Total partonic cross section written equivalently as

$$\begin{aligned}
\hat{\sigma}_{ij}(\hat{s}, m_Q^2, \mu^2) &= \int d\hat{t}\, d\hat{u}\, \hat{s}^2 \frac{d^2\hat{\sigma}_{ij}(\hat{s}, \hat{t}, \hat{u})}{d\hat{t} d\hat{u}} \\
\hat{s}^2 \frac{d^2\hat{\sigma}_{ij}^{(0)}(\hat{s}, \hat{t}, \hat{u})}{d\hat{t} d\hat{u}} &= \delta(\hat{s} - \hat{t} - \hat{u} - 2m_Q^2)\hat{\sigma}_{ij}^{B}(\hat{s}, \hat{t}, \hat{u})
\end{aligned}$$

Evaluating the Total Hadronic Cross Sections

Hadronic cross section obtained by convoluting the perturbative partonic cross section with the nonperturbative parton densities

$$\sigma_{pp}(s, m_Q^2) = \sum_{i,j=q,\overline{q},g} \int_{4m_Q^2/s}^{1} \frac{d\tau}{\tau} \, \delta(x_1 x_2 - \tau) \, F_i^p(x_1, \mu^2) F_j^p(x_2, \mu^2) \, \hat{\sigma}_{ij}(\tau, m_Q^2, \mu^2)$$

Some details

- Most NLO (and higher order) evaluations of the cross sections use NLO parton densities and two-loop calculations of α_s at LO and NLO and ...
- This is done to show the effects of the next order correction under the same conditions–also makes easier bookkeeping
- Our update here is NLO alone, further higher order calculations not valid far from threshold
- We compare our NLO calculations to $Q\overline{Q}$ production data by treating the quark mass, m, and scale, μ, as parameters
- After fixing the parameters for c and b, we extend these calculations to LHC energies
- We also use these same parameters to calculate quarkonium production in the color evaporation model at NLO

Charm Production Data as a Function of Mass and Scale

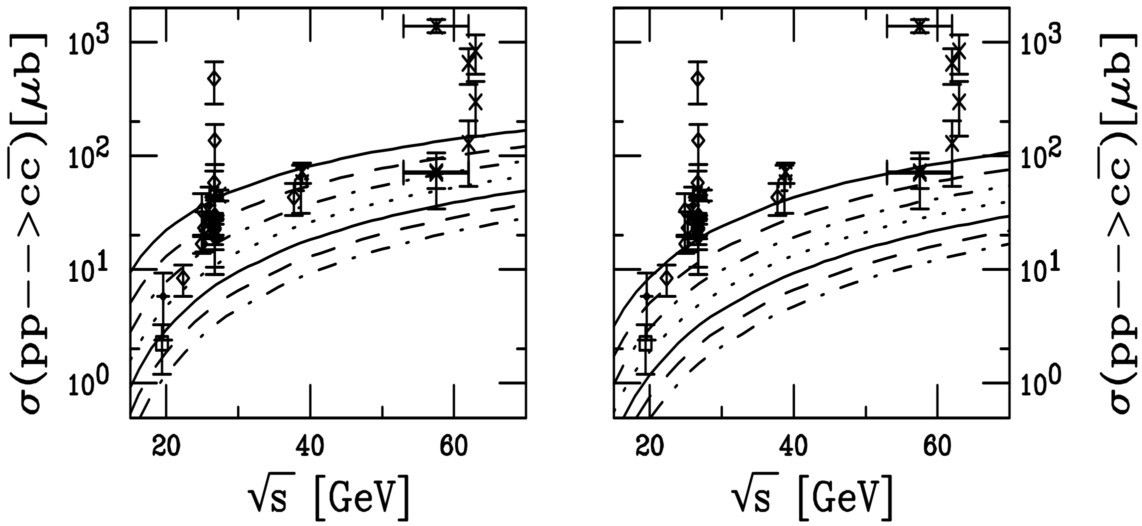

Figure 1: Total $c\bar{c}$ cross sections in pp interactions up to ISR energies as a function of the charm quark mass. All calculations are fully NLO using the MRST HO (central gluon) parton densities. The left-hand plot shows the results with the renormalization and factorization scales equal to the m_c while in the right-hand plot the scale is set to $2m_c$. From top to bottom the curves are $m_c = 1.2$, 1.3, 1.4, 1.5, 1.6, 1.7, and 1.8 GeV.

‘Best’ Agreement Found for Several Cases

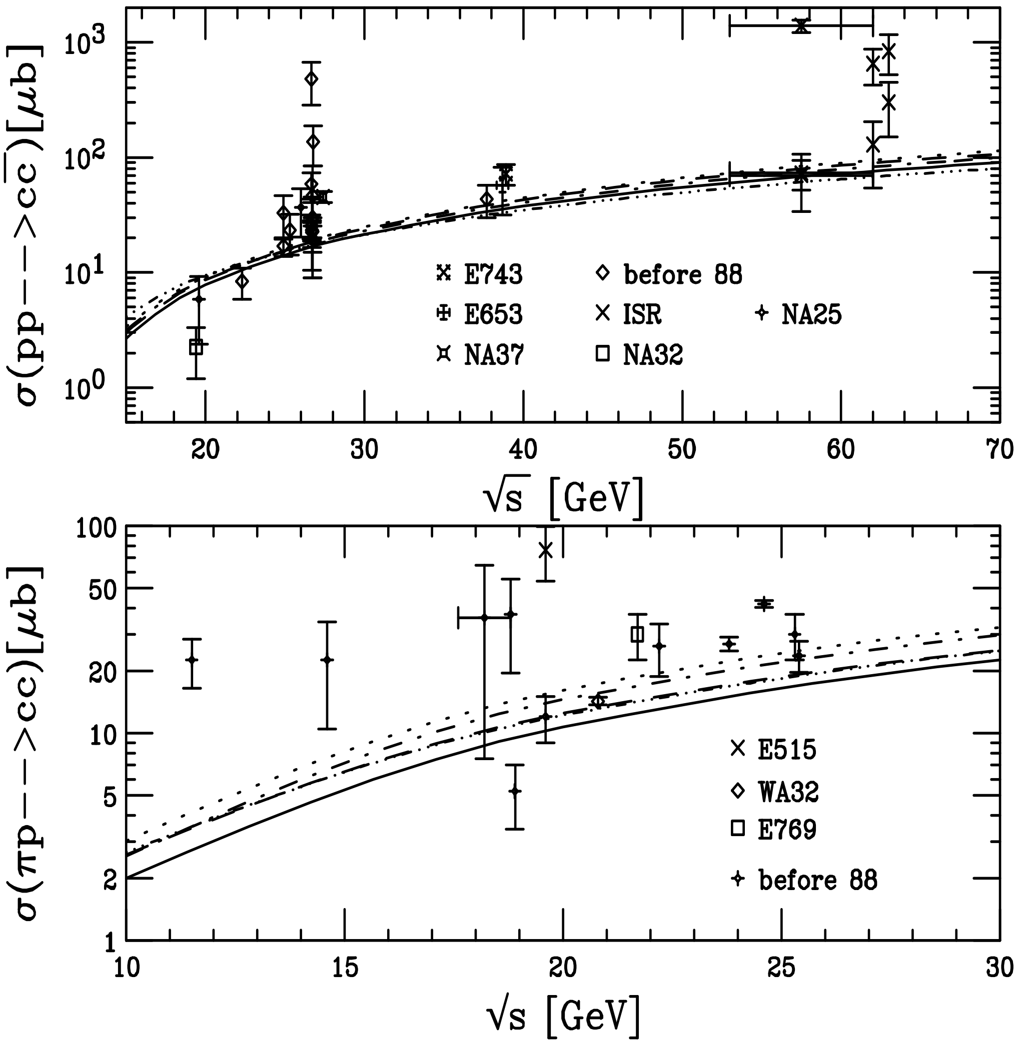

Figure 2: Total $c\bar{c}$ cross sections in pp and $\pi^- p$ interactions compared to data. All calculations are fully NLO. The curves are: MRST HO (central gluon) with $\mu = m = 1.4$ GeV (solid) and $\mu = 2m = 2.4$ GeV (dashed); CTEQ 5M with $\mu = m = 1.4$ GeV (dot-dashed) and $\mu = 2m = 2.4$ GeV (dotted); and GRV 98 HO with $\mu = m = 1.3$ GeV.

‘Best’ Extrapolated to LHC

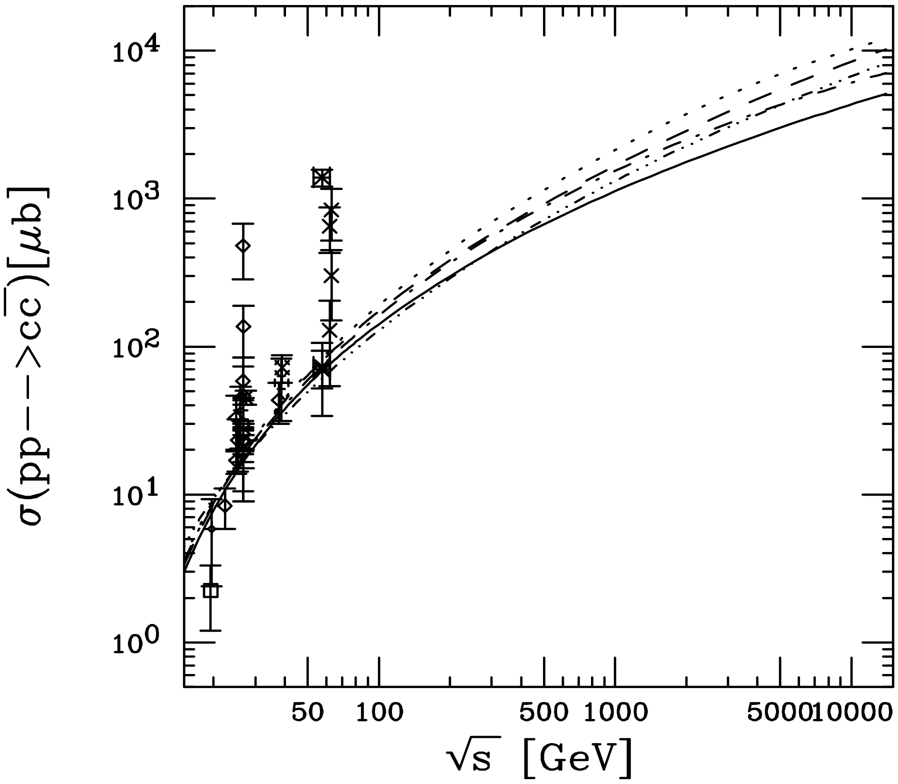

Figure 3: Total $c\bar{c}$ cross sections in pp interactions up to 14 TeV. All calculations are fully NLO. The curves are: MRST HO (central gluon) with $\mu = m = 1.4$ GeV (solid) and $\mu = 2m = 2.4$ GeV (dashed); CTEQ 5M with $\mu = m = 1.4$ GeV (dot-dashed) and $\mu = 2m = 2.4$ GeV (dotted); and GRV 98 HO with $\mu = m = 1.3$ GeV.

Bottom Production Data as a Function of Mass and Scale

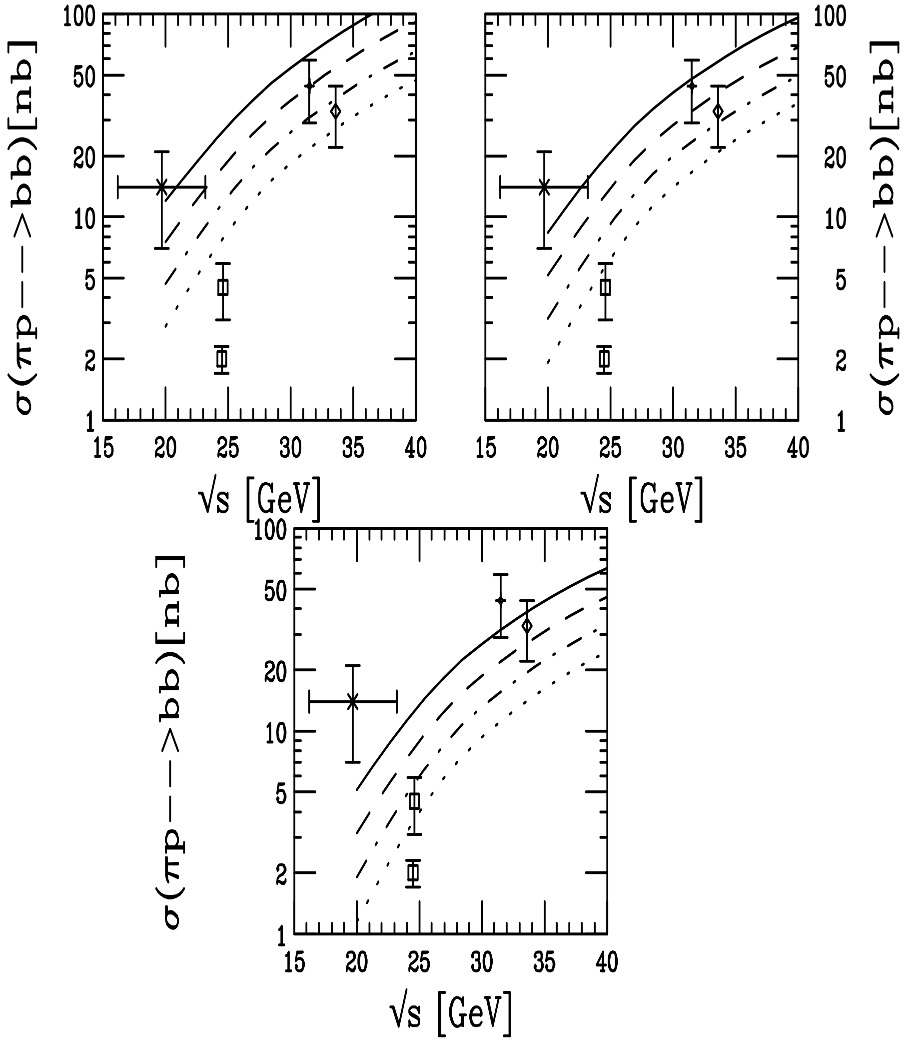

Figure 4: Total $b\bar{b}$ cross sections in $\pi^- p$ interactions at fixed-target energies as a function of the bottom quark mass. All calculations are fully NLO using the MRST HO (central gluon) parton densities. From the upper left, the plots show results with the renormalization and factorization scales equal to $m_b/2$, m_b and $2m_b$ respectively. In each plot, from top to bottom the curves are $m_b = 4.25$, 4.5, 4.75, and 5 GeV.

Sparse Data for Bottom

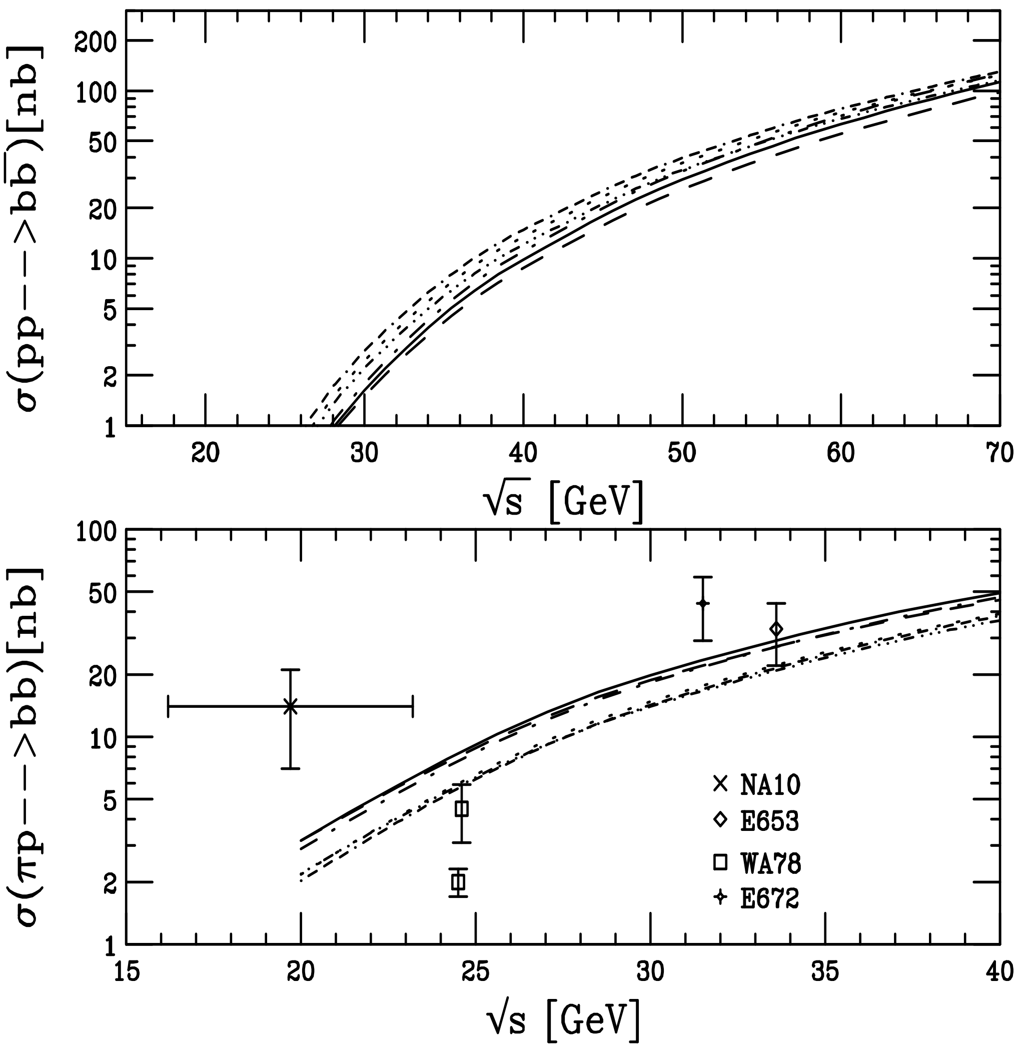

Figure 5: Total $b\bar{b}$ cross sections in pp and $\pi^- p$ interactions compared to data. All calculations are fully NLO. The curves are: MRST HO (central gluon) with $\mu = m = 4.75$ GeV (solid), $\mu = 2m = 9$ GeV (dashed), and $\mu = m/2 = 2.5$ GeV (dot-dashed); as well as the GRV 98 HO distributions with $\mu = m = 4.75$ GeV (dotted), $\mu = 2m = 9$ GeV (dotted), and $\mu = m/2 = 2.5$ GeV.

HERA-B Preliminary Measurement Suggests NLO Calculations Alone Miss Most of b Cross Section

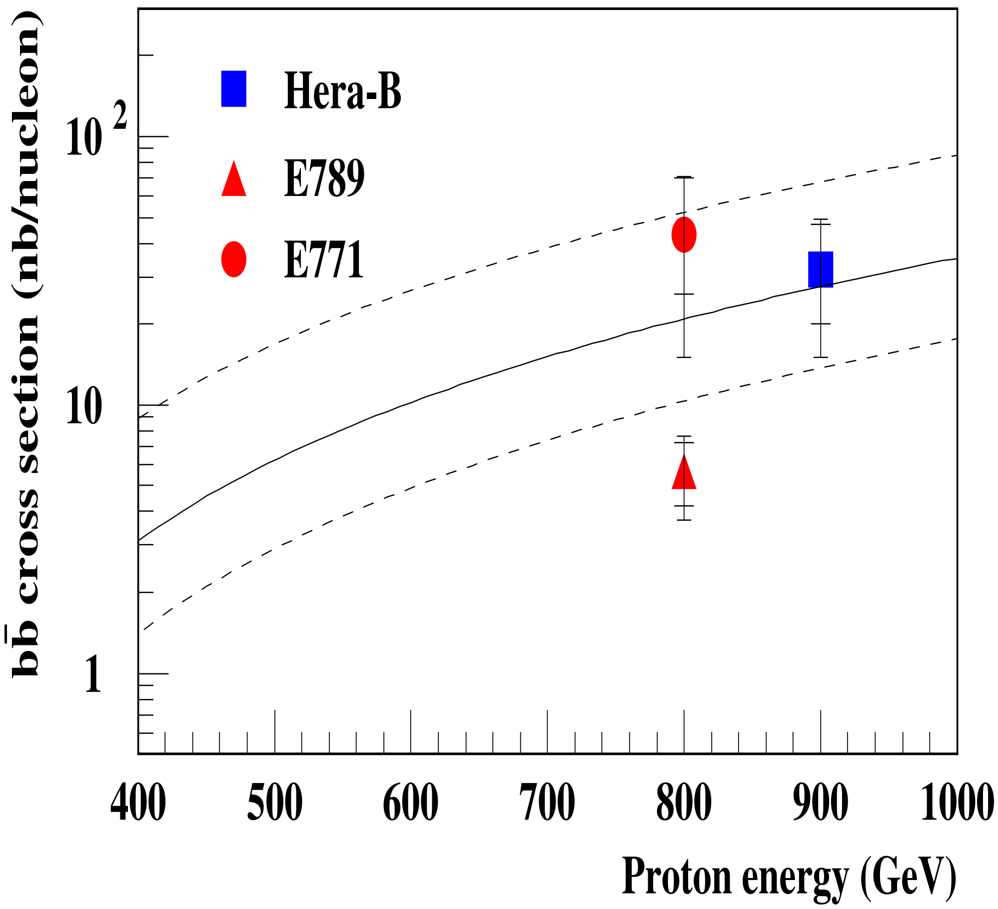

Figure 6: Total $b\bar{b}$ cross sections in pp interactions compared to data. The curves are of order NNLO-NNLL with a band of uncertainties due to kinematics and scale. The calculations (N. Kidonakis, E. Laenen, S. Moch and R.V., Phys. Rev. **D64** (2001) 114001) are done with the CTEQ5M densities and $m_b = 4.75$ GeV.

Extrapolation to LHC

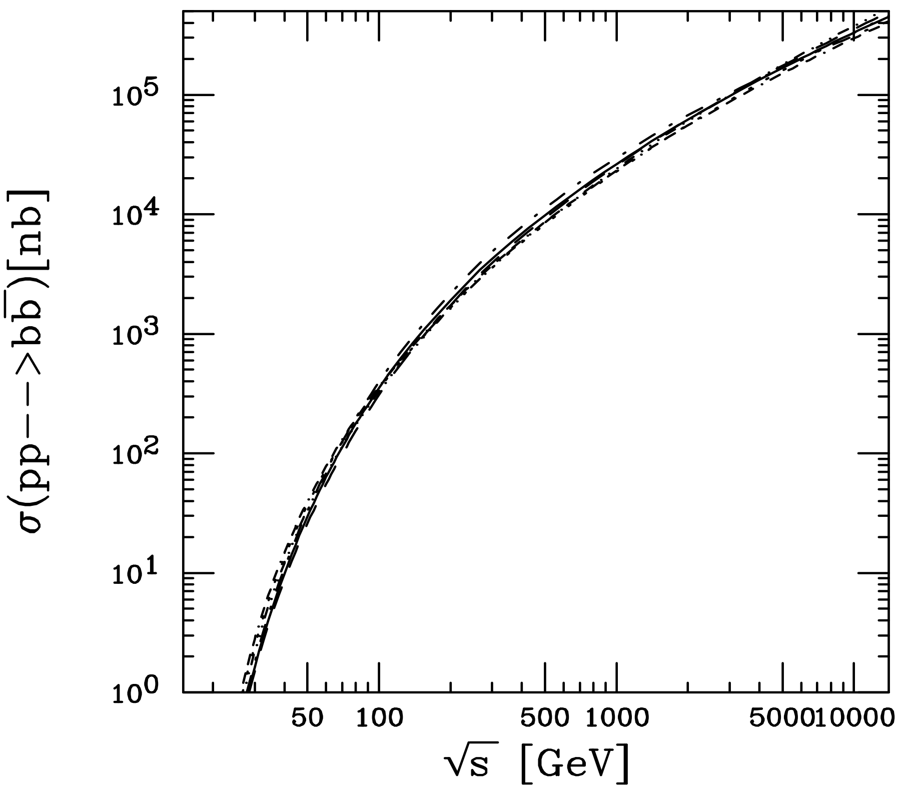

Figure 7: Total $b\bar{b}$ cross sections in pp interactions up to 14 TeV. All calculations are fully NLO. The curves are: MRST HO (central gluon) with $\mu = m = 4.75$ GeV (solid), $\mu = 2m = 9$ GeV (dashed), and $\mu = m/2 = 2.5$ GeV (dot-dashed); as well as the GRV 98 HO distributions with $\mu = m = 4.75$ GeV (dotted), $\mu = 2m = 9$ GeV (dotted), and $\mu = m/2 = 2.5$ GeV.

Effects of Fragmentation and Intrinsic k_T on Distributions

Double differential cross sctions

$$s^2\frac{d^2\sigma_{pp}(s,t,u)}{dtdu} = \sum_{i,j=q,\overline{q},g}\int_{x_1^-}^1 \frac{dx_1}{x_1}\int_{x_2^-}^1 \frac{dx_2}{x_2} f_i^p(x_1,\mu^2) f_j^p(x_2,\mu^2)\mathcal{J}_K(\hat{s},\hat{t},\hat{u})\hat{s}^2\frac{d^2\hat{\sigma}_{ij}(\hat{s},\hat{t},\hat{u})}{d\hat{t}d\hat{u}}$$

$f_i^p = F_i^p/x$ is parton density, $\mathcal{J}_K$ is a kinematics-dependent Jacobian

In these calculations, we include intrinsic transverse momentum and fragmentation, needed to smear the pair p_T and ϕ distributions as measured for $D\overline{D}$ correlations (Peterson fragmentation and $k_T^2 = 1$ GeV^2 cancel each other in the single D p_T distribution)

Adds the following extra integrations:

$$\int dz_3 dz_4 d^2k_{T1} d^2k_{T2} \frac{D_{H/Q}(z_3,\mu^2)}{z_3}\frac{D_{\overline{H}/\overline{Q}}(z_4,\mu^2)}{z_4} g_p(k_{T1}) g_p(k_{T2})$$

Fragmentation function a la Peterson

$$D_{H/Q}(z) = \frac{N}{z(1-1/z-\epsilon_Q/(1-z))^2}$$

$\epsilon_Q = 0.06$ for charm, 0.006 for bottom, normalized so that $\Sigma_H \int D_{H/Q}(z)dz = 1$ for all heavy flavored hadrons

Gaussian k_T smearing

$$g_p(k_T) = \frac{1}{\pi\langle k_T^2\rangle_p}\exp(-k_T^2/\langle k_T^2\rangle_p) \tag{1}$$

Nuclear Effects on p_T Broadening

Additional broadening–beyond the intrinsic broadening–assumed to arise from multiple parton scattering in the target before hard interaction

J/ψ, Υ and Drell-Yan show effects of broadening in pA, parameterized as

$$\langle k_T^2 \rangle_{iA} = \langle k_T^2 \rangle_{pp} + (\langle \nu \rangle - 1)\Delta^2(\mu)$$

The broadening is proportional to the average number of collisions of the projectile parton in the target,

$$\langle \nu \rangle = \sigma_{NN} \frac{\int d^2b T_A^2(b)}{\int d^2b T_A(b)} = \frac{3}{2}\sigma_{NN}\rho_0 R_A$$

$T_A(b)$ is the nuclear profile function

The second equality is average over impact parameter assuming a sperical nucleus, $\rho_0 = 0.16$ fm^{-3} is the central nuclear density and R_A is the nuclear radius

Δ^2, the strength of the broadening, depends on the scale of the interactions

$$\Delta^2(\mu) = 0.225 \frac{\ln^2(\mu/\mathrm{GeV})}{1 + \ln(\mu/\mathrm{GeV})} \mathrm{GeV}^2$$

$\Delta^2(\mu)$ evaluated at $2m_Q$, larger for bottom than charm, actually opposite the effect on J/ψ and Υ

$(\langle \nu \rangle - 1)\Delta^2(\mu)$ (GeV^2)		
$Q\overline{Q}$	pA	central AA
$c\overline{c}$	0.35	0.7
$b\overline{b}$	1.57	3.14

Total $\langle k_T^2 \rangle_{AA}$ obtained by including $\langle k_T^2 \rangle_{pp} = 1$ GeV^2

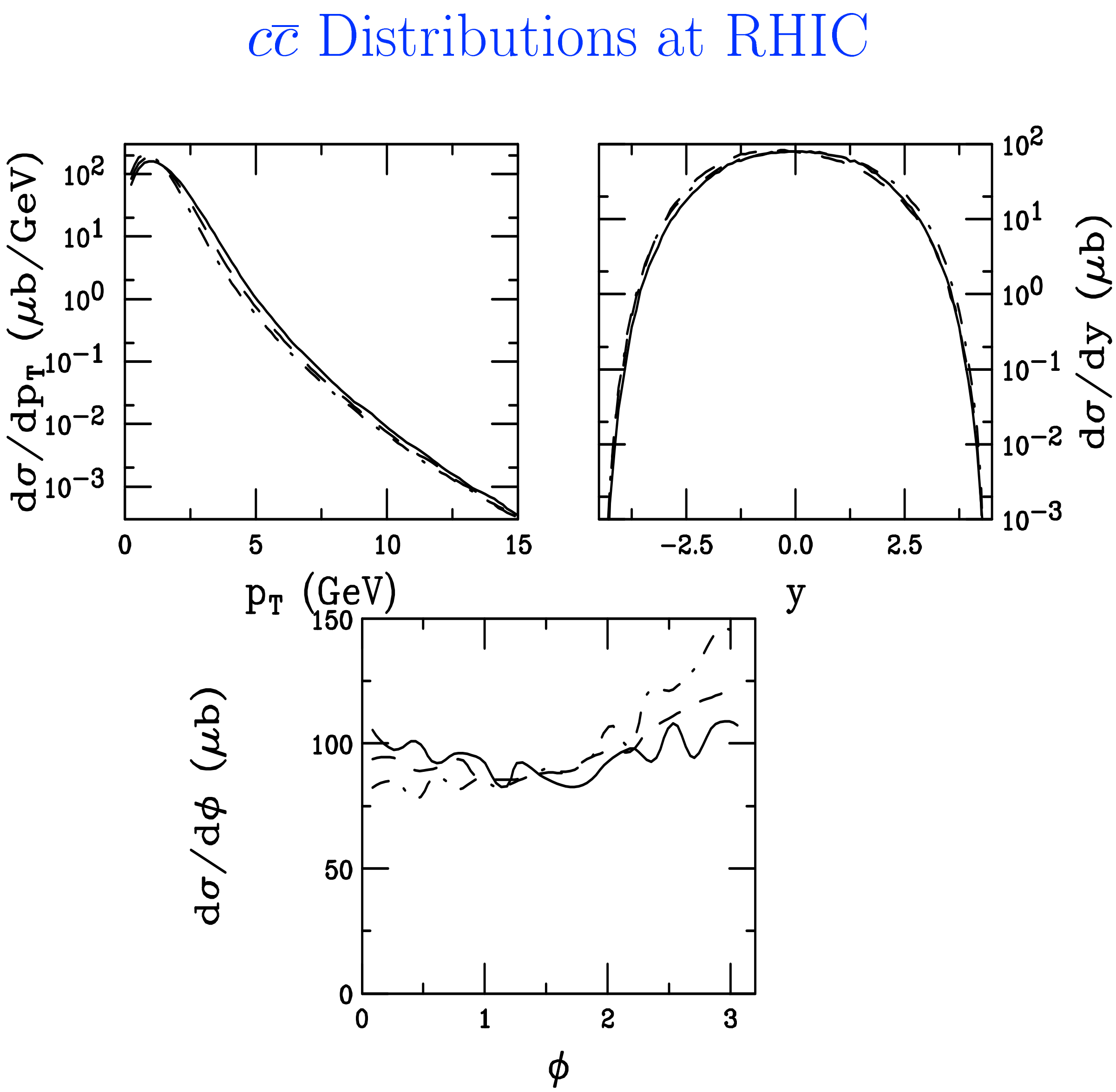

Figure 8: Exclusive NLO $c\overline{c}$ pair production in pp, pA and AA interactions at $\sqrt{s} = 200$ GeV as a function of p_T, y, and ϕ. The per nucleon cross section is given for pA and AA interactions. The dot-dashed curves are the pp results, the dashed curves are the pA results, and the solid curves are the AA results.

Single Charm Distributions at RHIC

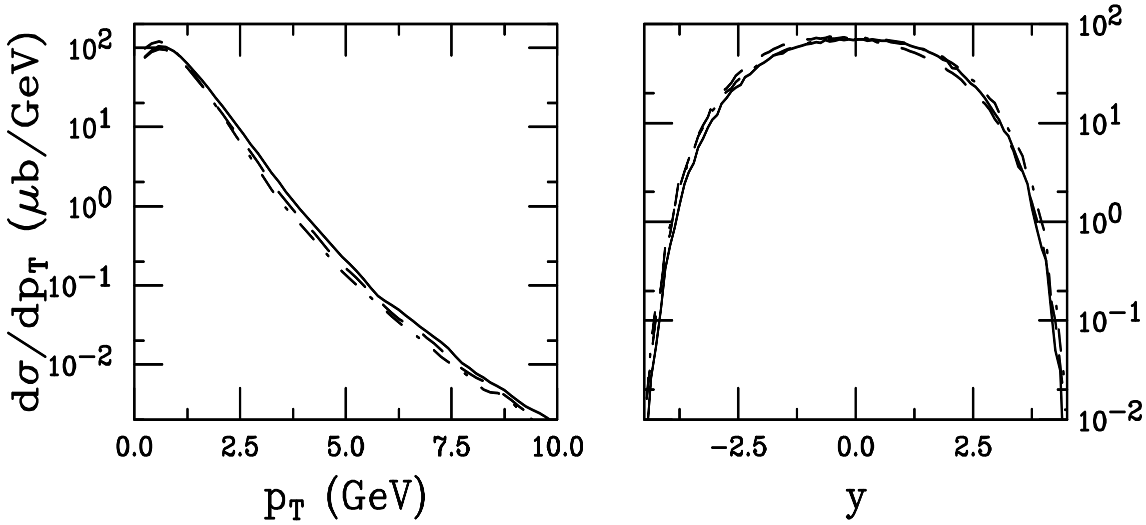

Figure 9: Inclusive NLO c quark production in pp, pA and AA interactions at $\sqrt{s} = 200$ GeV as a function of p_T and y. The p_T distributions are integrated over $x_F > 0$ only. The per nucleon cross section is given for pA and AA interactions. The dot-dashed curves are the pp results, the dashed curves are the pA results, and the solid curves are the AA results.

Single Charm at RHIC: pA/pp

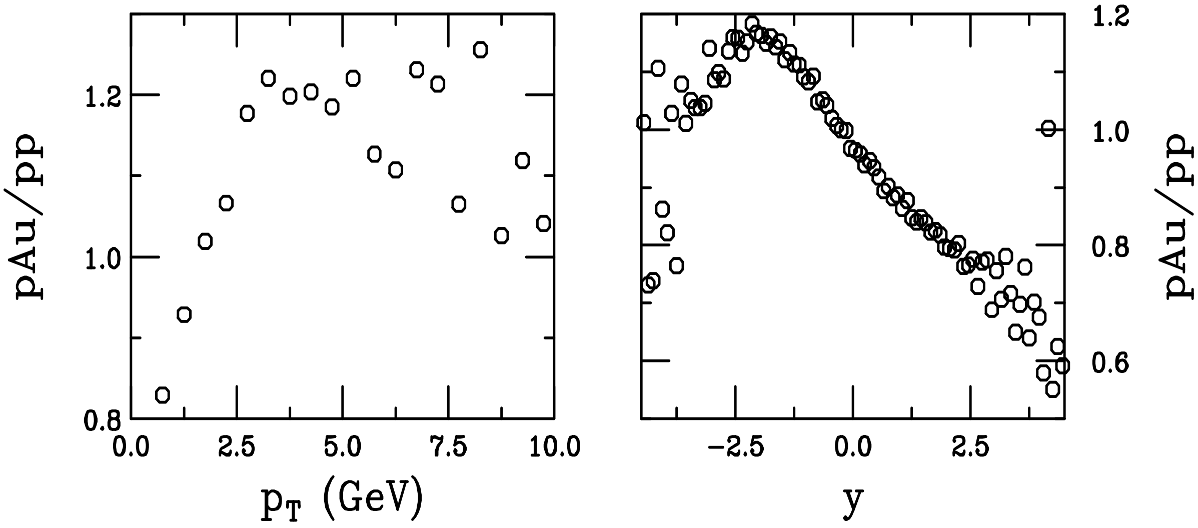

Figure 10: The ratio of pA to pp inclusive NLO c quark production at $\sqrt{s} =$ 200 GeV as a function of p_T and y.

Single Charm at RHIC: AA/pp

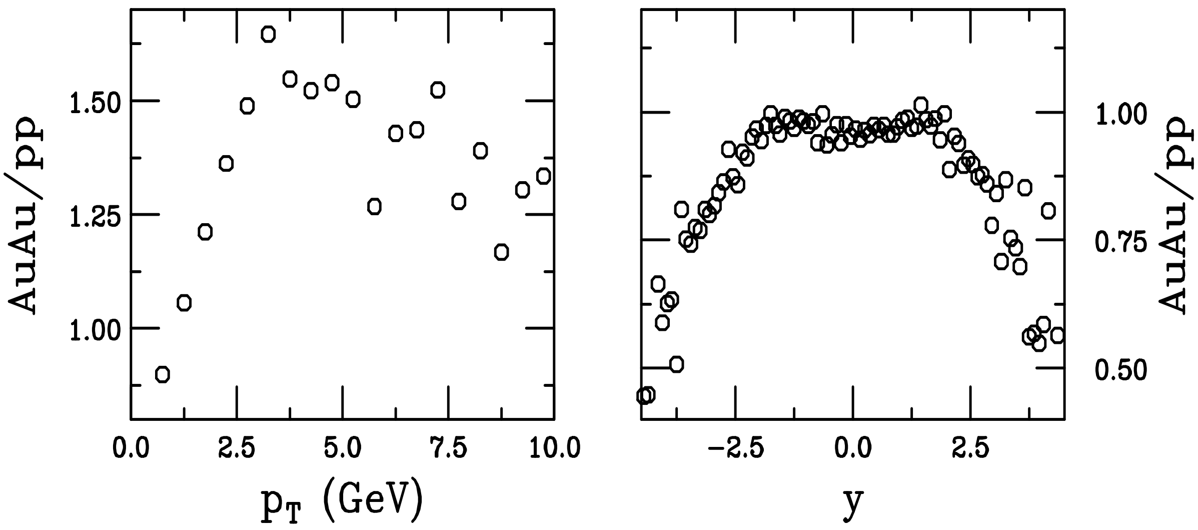

Figure 11: The ratio of AA to pp inclusive NLO c quark production at $\sqrt{s} = 200$ GeV as a function of p_T and y.

$b\bar{b}$ Distributions at RHIC

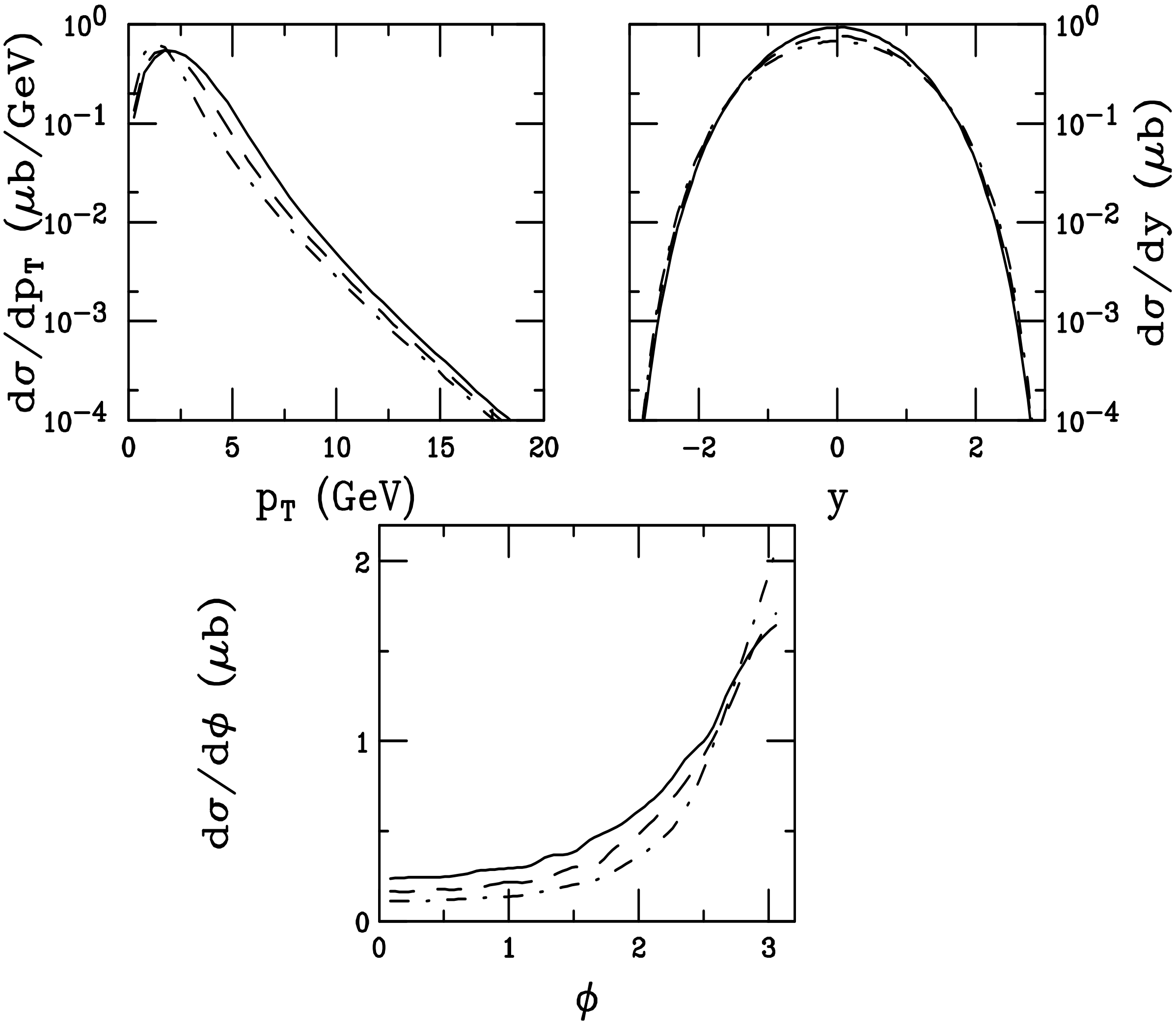

Figure 12: Exclusive NLO $b\bar{b}$ pair production in pp, pA and AA interactions at $\sqrt{s} = 200$ GeV as a function of p_T, y, and ϕ. The per nucleon cross section is given for pA and AA interactions. The per nucleon cross section is given for pA and AA interactions. The dot-dashed curves are the pp results, the dashed curves are the pA results, and the solid curves are the AA results.

Single Bottom Quark Distributions at RHIC

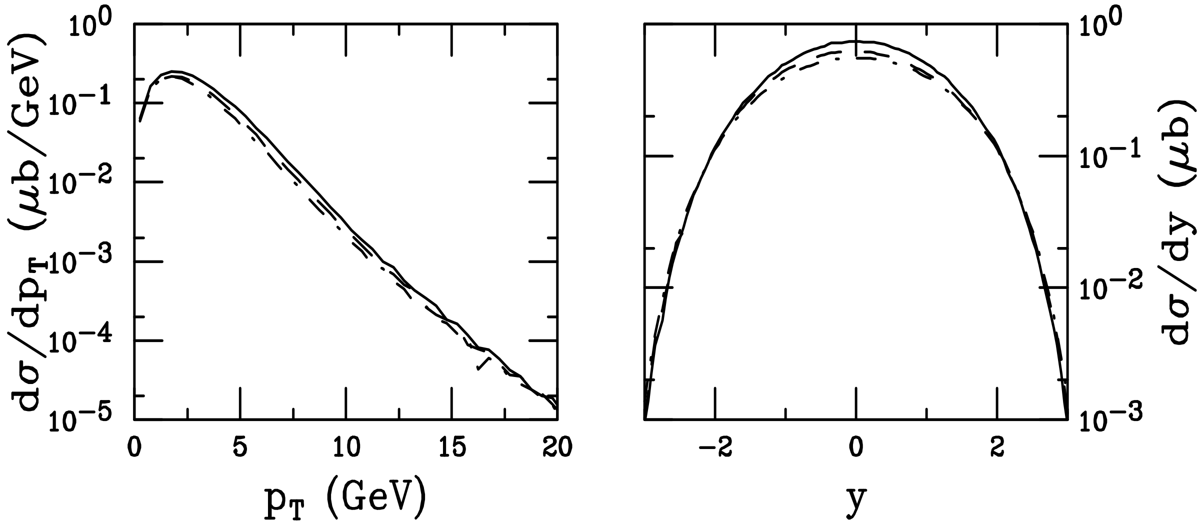

Figure 13: Inclusive NLO b quark production in pp, pA and AA interactions at $\sqrt{s} = 200$ GeV as a function of p_T and y. The p_T distributions are integrated over $x_F > 0$ only. The per nucleon cross section is given for pA and AA interactions. The dot-dashed curves are the pp results, the dashed curves are the pA results, and the solid curves are the AA results.

Single Bottom at RHIC: pA/pp

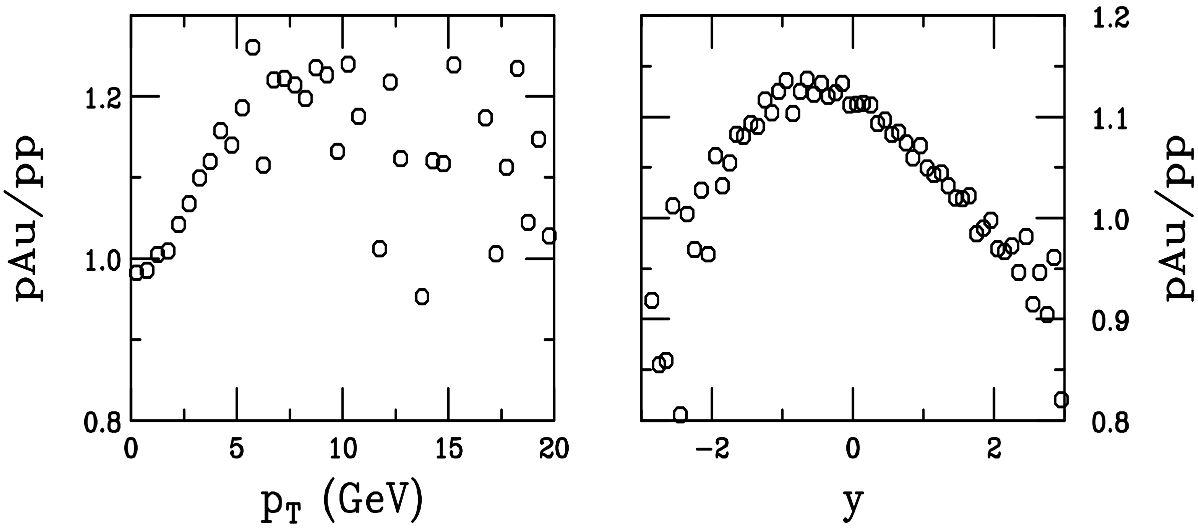

Figure 14: The ratio of pA to pp inclusive NLO b quark production at $\sqrt{s} =$ 200 GeV as a function of p_T and y.

Single Bottom at RHIC: AA/pp

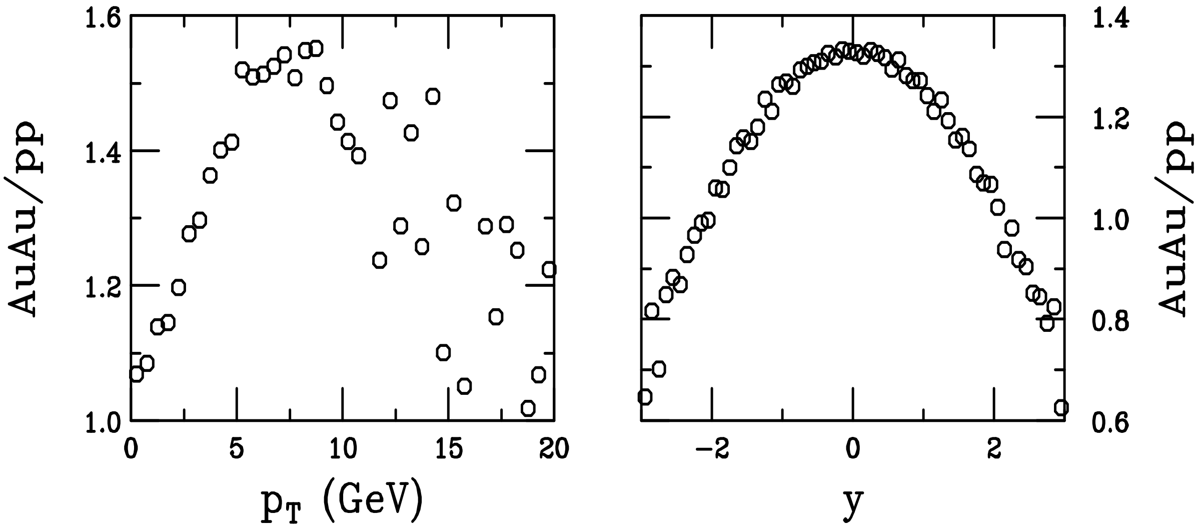

Figure 15: The ratio of AA to pp inclusive NLO b quark production at $\sqrt{s} = 200$ GeV as a function of p_T and y.

Single Charm Distributions at LHC

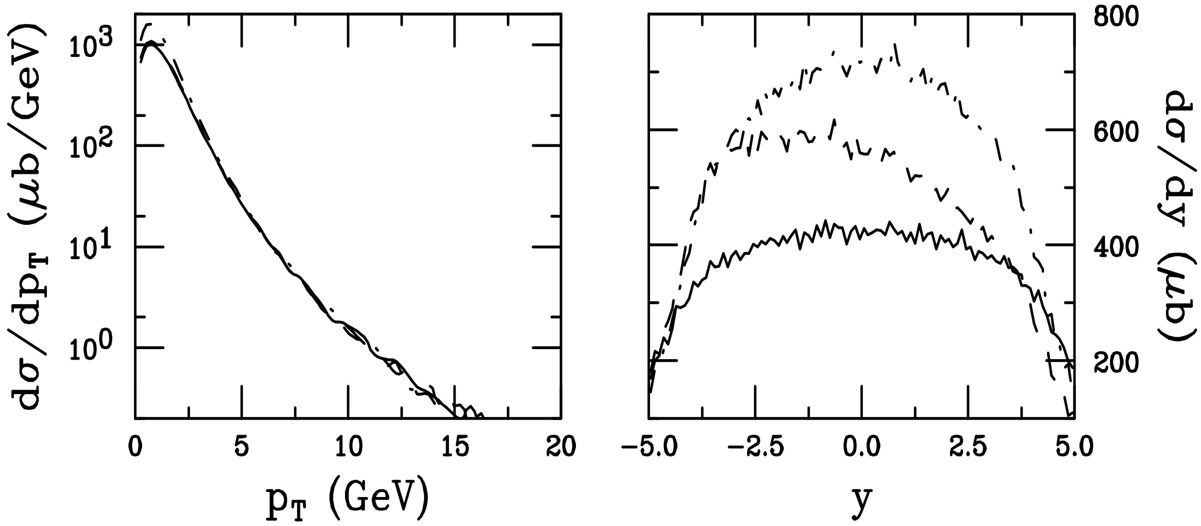

Figure 16: Inclusive NLO c quark production in pp, pA and AA interactions at $\sqrt{s} = 5.5$ TeV as a function of p_T and y. The p_T distributions are integrated over $x_F > 0$ only. The per nucleon cross section is given for pA and AA interactions. The dot-dashed curves are the pp results, the dashed curves are the pA results, and the solid curves are the AA results.

Single Charm at LHC: pA/pp

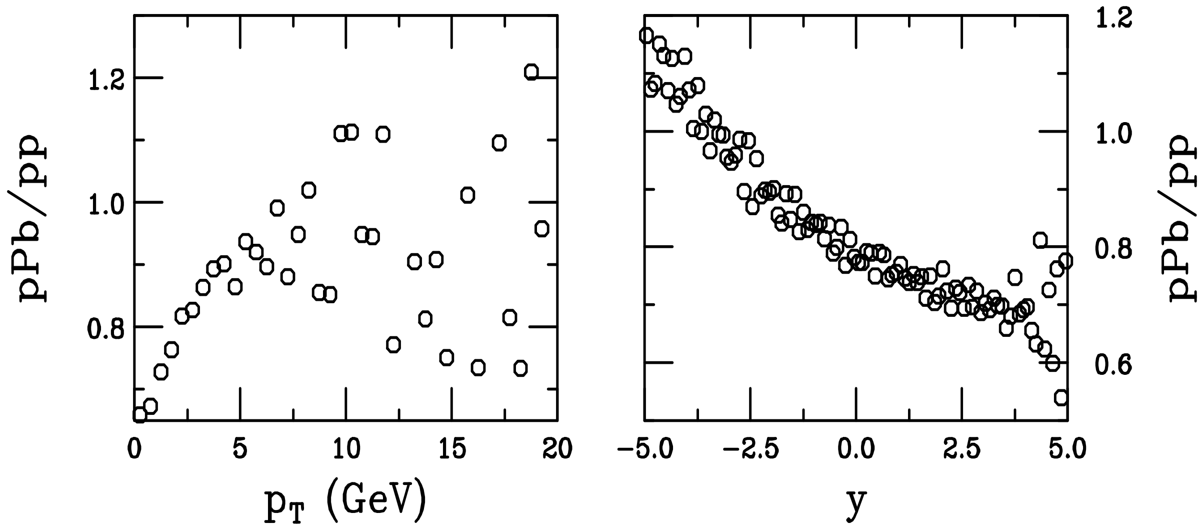

Figure 17: The ratio of pA to pp inclusive NLO c quark production at $\sqrt{s} =$ 5.5 TeV as a function of p_T and y.

Single Charm at LHC: AA/pp

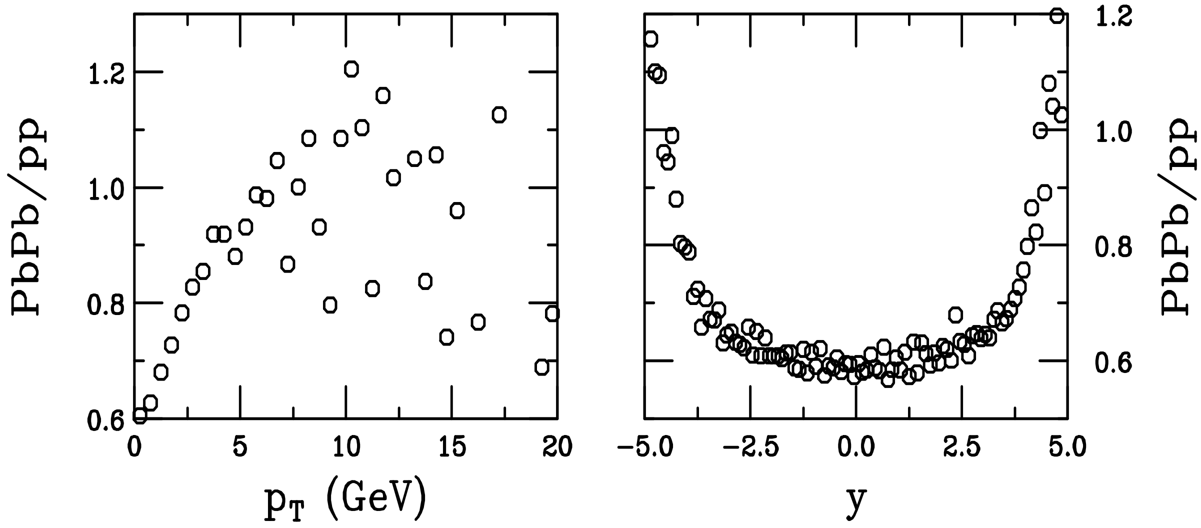

Figure 18: The ratio of AA to pp inclusive NLO c quark production at $\sqrt{s} = 5.5$ TeV as a function of p_T and y.

Single Bottom Distributions at LHC

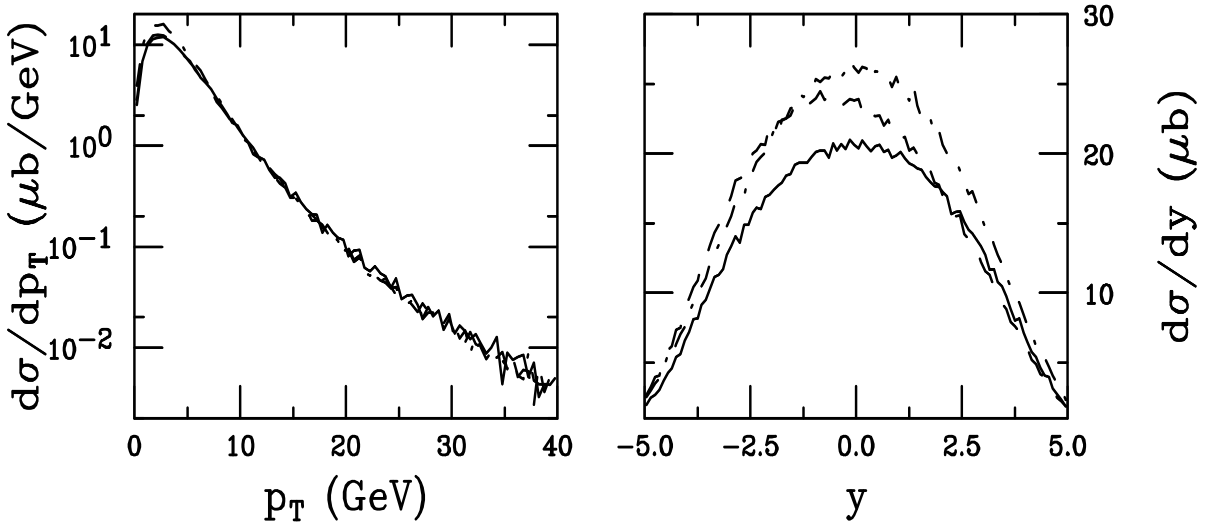

Figure 19: Inclusive NLO b quark production in pp, pA and AA interactions at $\sqrt{s} = 5.5$ TeV as a function of p_T and y. The p_T distributions are integrated over $x_F > 0$ only. The per nucleon cross section is given for pA and AA interactions. The dot-dashed curves are the pp results, the dashed curves are the pA results, and the solid curves are the AA results.

Single Bottom at LHC: pA/pp

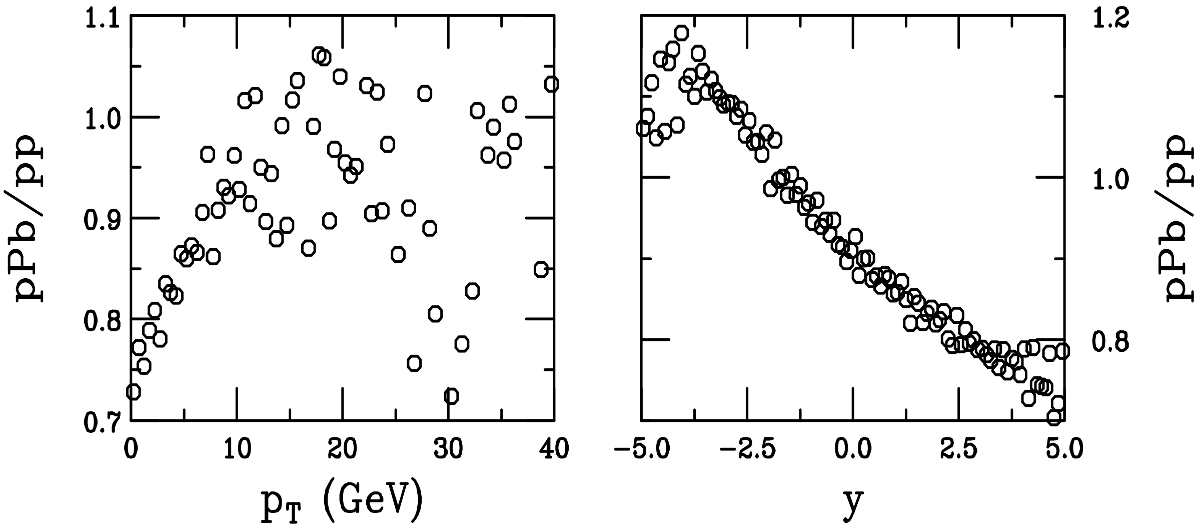

Figure 20: The ratio of pA to pp inclusive NLO b quark production at $\sqrt{s} = 5.5$ TeV as a function of p_T and y.

Single Bottom at LHC: AA/pp

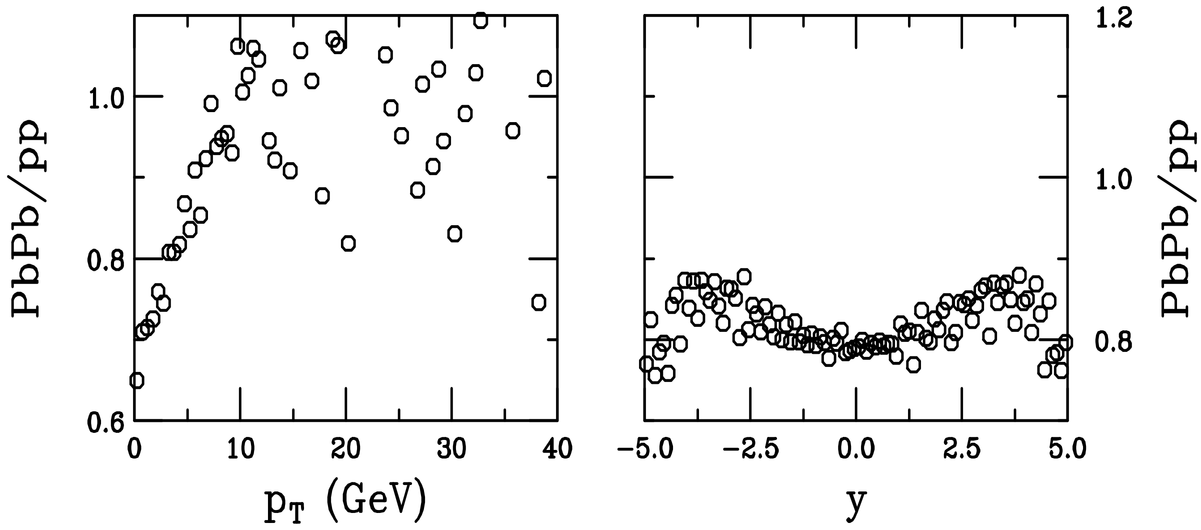

Figure 21: The ratio of AA to pp inclusive NLO b quark production at $\sqrt{s} = 5.5$ TeV as a function of p_T and y.

Quarkonium Production in the CEM

All quarkonium states are treated like $Q\overline{Q}$ below $H\overline{H}$ (heavy meson) threshold

Distributions for all quarkonium family members identical

At LO, $gg \to Q\overline{Q}$ and $q\overline{q} \to Q\overline{Q}$; NLO add $gq \to Q\overline{Q}q$

$$\sigma_Q^{\rm CEM} = F_Q \sum_{i,j} \int_{4m_Q^2}^{4m_H^2} d\hat{s} \int dx_1 dx_2 \; f_{i/p}(x_1,Q^2) \; f_{j/p}(x_2,Q^2) \; \hat{\sigma}_{ij}(\hat{s}) \; \delta(\hat{s} - x_1 x_2 s)$$

F_Q fixed at NLO

Data and branching ratios can be used to separate out the F_Q's for each state in quarkonium family

Range of m_Q, Q^2, and parton densities fixed from open $Q\overline{Q}$ productiion

Production and Feeddown Fractions

Resonance	$\sigma_i^{\rm dir}/\sigma_H$	f_i
J/ψ	0.62	0.62
ψ'	0.14	0.08
χ_{c1}	0.6	0.16
χ_{c2}	0.99	0.14
Υ	0.52	0.52
Υ'	0.33	0.10
Υ''	0.20	0.02
$\chi_b(1P)$	1.08	0.26
$\chi_b(2P)$	0.84	0.10

Table 1: The ratios of the direct quarkonium production cross sections, $\sigma_i^{\rm dir}$, to the inclusive J/ψ and Υ cross sections, denoted σ_H, and the feeddown contributions of all states to the J/ψ and Υ cross sections, f_i.

J/ψ Production Cross Sections vs. Forward Data

Forward J/ψ cross sections compared to data up to 63 GeV

GRV 98 result has different energy dependence

Inclusive J/ψ cross section–all figures include feeddown from χ_c and ψ'

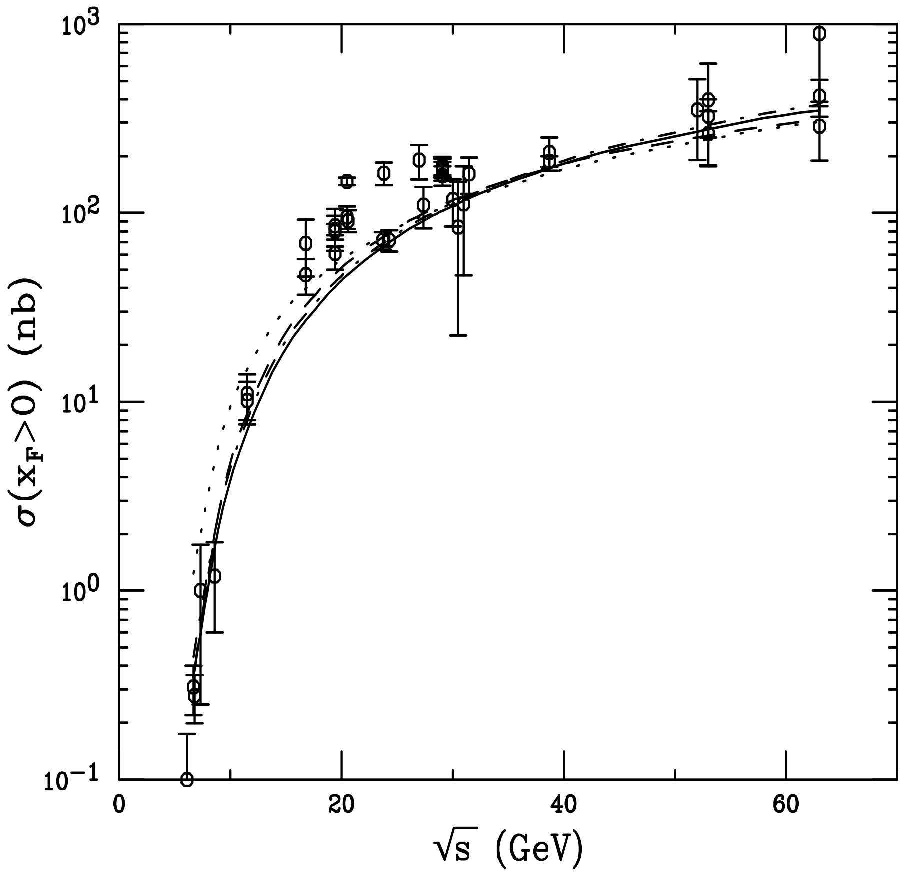

Figure 22: J/ψ production data on total cross sections with $x_F > 0$ compared to NLO CEM calculations. The solid curve employs the MRST HO distributions with $m_c = \mu/2 = 1.2$ GeV, the dashed, MRST HO with $m_c = \mu = 1.4$ GeV, the dot-dashed, CTEQ 5M with $m_c = \mu/2 = 1.2$ GeV, and the dotted, GRV 98 HO with $m_c = \mu = 1.3$ GeV.

J/ψ Production Cross Sections at $y = 0$

J/ψ cross sections compared to $y = 0$ data

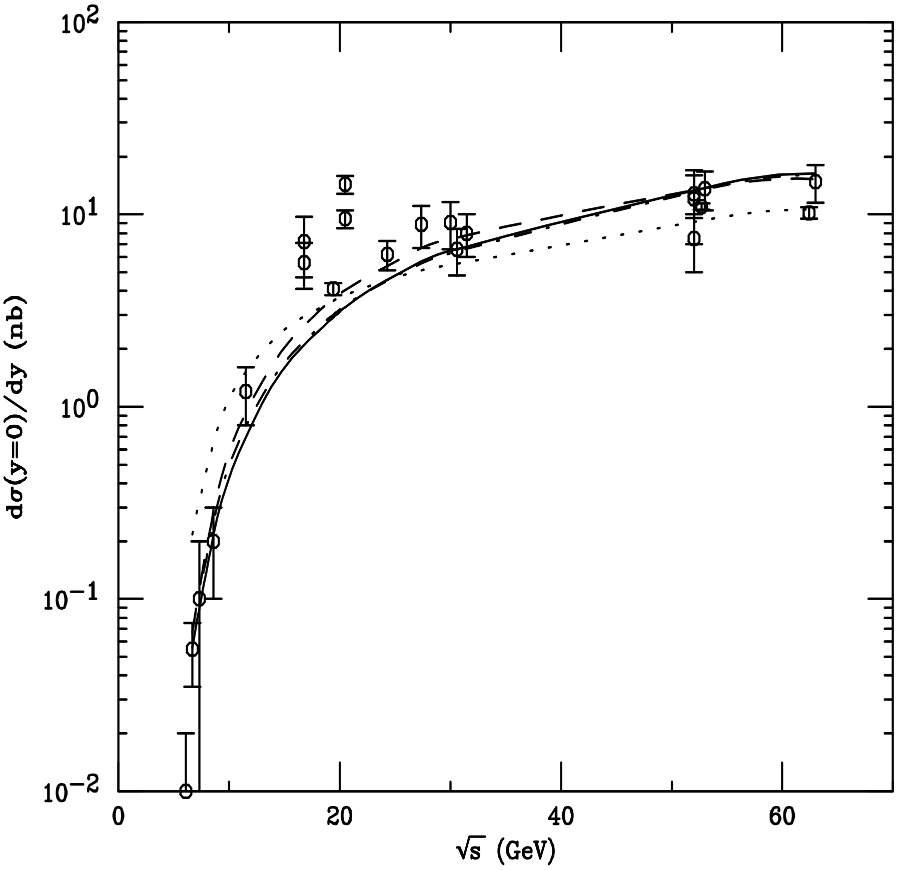

Figure 23: J/ψ production data at $y = 0$ compared to NLO CEM calculations. The solid curve employs the MRST HO distributions with $m_c = \mu/2 = 1.2$ GeV, the dashed, MRST HO with $m_c = \mu = 1.4$ GeV, the dot-dashed, CTEQ 5M with $m_c = \mu/2 = 1.2$ GeV, and the dotted, GRV 98 HO with $m_c = \mu = 1.3$ GeV.

J/ψ Total Cross Sections Extrapolated to LHC

Total forward J/ψ cross sections extrapolated to LHC

Energy dependence obtained from NLO $c\bar{c}$ cross section below the $D\overline{D}$ threshold

Less than a factor of two between results at 5.5 TeV

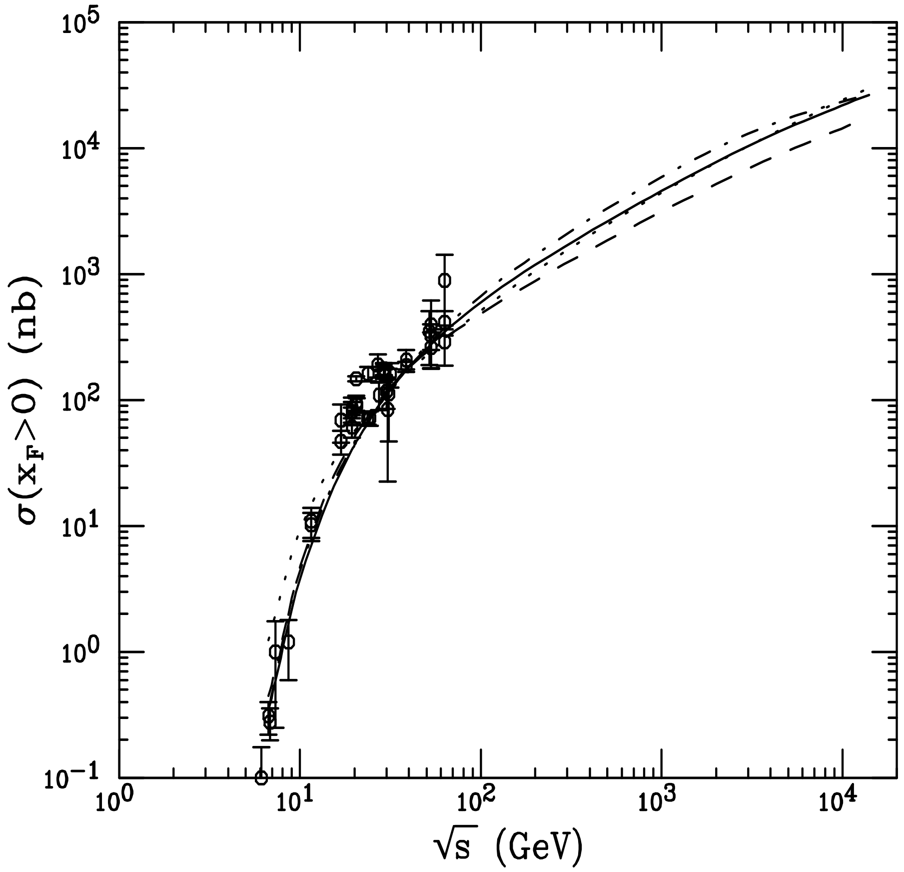

Figure 24: J/ψ forward cross sections calculated to NLO in the CEM. The solid curve employs the MRST HO distributions with $m_c = \mu/2 = 1.2$ GeV, the dashed, MRST HO with $m_c = \mu = 1.4$ GeV, the dot-dashed, CTEQ 5M with $m_c = \mu/2 = 1.2$ GeV, and the dotted, GRV 98 HO with $m_c = \mu = 1.3$ GeV.

Fitted Fractions and Cross Sections for J/ψ in CEM

Case	PDF	m_c (GeV)	μ/m_c	$\sigma_{J/\psi}/\sigma_c^{\rm CEM}$
$\psi1$	MRST HO	1.2	2	0.0154
$\psi2$	MRST HO	1.4	1	0.0272
$\psi3$	CTEQ 5M	1.2	2	0.0155
$\psi4$	GRV 98 HO	1.3	1	0.0229

Table 2: The production fractions obtained from fitting the CEM cross section to the J/ψ total cross sections and $y = 0$ cross sections as a function of energy. The PDF, charm quark mass, and scales used are the same as those obtained by comparison of the $c\overline{c}$ cross section to the pp data.

Case	$\sigma_{J/\psi}^{\rm tot}$	$\sigma_{J/\psi}^{\rm dir}$	$\sigma_{\chi_c \rightarrow J/\psi}$	$\sigma_{\psi'}^{\rm dir}$
$\psi1$	30.8	19.0	9.2	4.3
$\psi2$	20.2	12.5	6.1	2.8
$\psi3$	36.0	22.2	10.8	5.0
$\psi4$	32.1	19.8	9.6	4.5

Table 3: The charmonium cross sections (in μb) obtained from the CEM fits for NN collisions at 5.5 TeV in each case. The production fractions above are them multiplied by the appropriate charmonium ratios determined from data.

Inclusive Υ Cross Sections at $y = 0$

Cross sections include all $\Upsilon(nS)$ states and their decays to muon pairs

Data is from pp interactions except for highest two points where only $p\overline{p}$ colliders available

At high energies, $gg \to Q\overline{Q}$ dominates and differences between $p\overline{p} \to \Upsilon$ and $pp \to \Upsilon$ are negliglble

LHC ion energy only a factor of 3 beyond Tevatron Run I

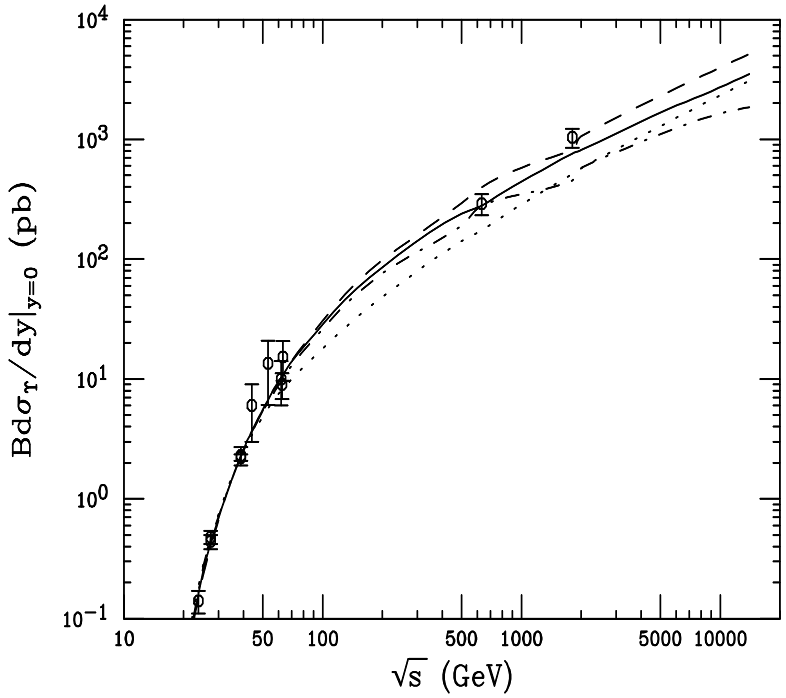

Figure 25: Inclusive Υ production data, combined from all three S states, and compared to NLO CEM calculations. The solid curve employs the MRST HO distributions with $m_b = \mu = 4.75$ GeV, the dashed, $m_b = \mu/2 = 4.5$ GeV, the dot-dashed, $m_b = 2\mu = 5$ GeV, and the dotted, GRV 98 HO with $m_b = \mu = 4.75$ GeV.

Fitted Fractions and Cross Sections for Υ in CEM

Case	PDF	m_b (GeV)	μ/m_b	$\sigma_{B\sum\Upsilon}/\sigma_b^{\rm CEM}$	$\sigma_\Upsilon/\sigma_b^{\rm CEM}$
Υ1	MRST HO	4.75	1	0.001014	0.0291
Υ2	MRST HO	4.50	2	0.000740	0.0212
Υ3	MRST HO	5.00	0.5	0.001876	0.0540
Υ4	GRV 98 HO	4.75	1	0.000787	0.0225

Table 4: The production fractions obtained from fitting the CEM cross section to the combined Υ cross sections to muon pairs at $y = 0$ as a function of energy. The PDF, charm quark mass, and scales used are the same as those obtained by comparison of the $b\overline{b}$ cross section to the $\pi^- p$ data.

Case	σ_Υ	$\sigma_{\Upsilon'}$	$\sigma_{\Upsilon''}$	$\sigma_{\chi_b(1P)}$	$\sigma_{\chi_b(2P)}$
Υ1	187	119	72	389	302
Υ2	259	164	99	537	418
Υ3	126	80	49	262	204
Υ4	145	92	56	302	235

Table 5: The direct bottomonium cross sections (in nb) obtained from the CEM fits for NN collisions at 5.5 TeV in each case above. The production fractions for the total Υ are multiplied by the appropriate ratios determined from data.

How Should the K Factor Be Defined?

Often it is most convenient to use leading order matrix elements in calculation: full higher order calculations unavailable; speed of computation; LO suitable for purposes; event generators

Most higher-order (NLO and beyond) calculations are to determine the size of the next-order correction, defining the theoretical 'K factor' as

$$K = \frac{\sigma(\text{full NLO})}{\sigma(\text{LO ME only})}$$

Thus in these evaluations, NLO parton densities are used with a two-loop evaluation of α_s

It is, however, more consistent to calculate the LO cross sections alone with LO parton densities and one-loop evaluations of α_s: LO parton densities are tuned to fit same data as NLO fits

However, it is then not reasonable to multiply the full LO calculations by the K factor obtained above, if the technology is available, better to define the K factor as

$$K = \frac{\sigma(\text{full LO}) + \sigma(\mathcal{O}(\alpha_s) \text{ corr at NLO})}{\sigma(\text{full LO})}$$

Another possibility:

$$K = \frac{\sigma(\text{full NLO})}{\sigma(\text{full LO})}$$

We compare the possible definitions of K

LO and NLO Parton Densities at $Q^2 = 4\ \mathrm{GeV}^2$

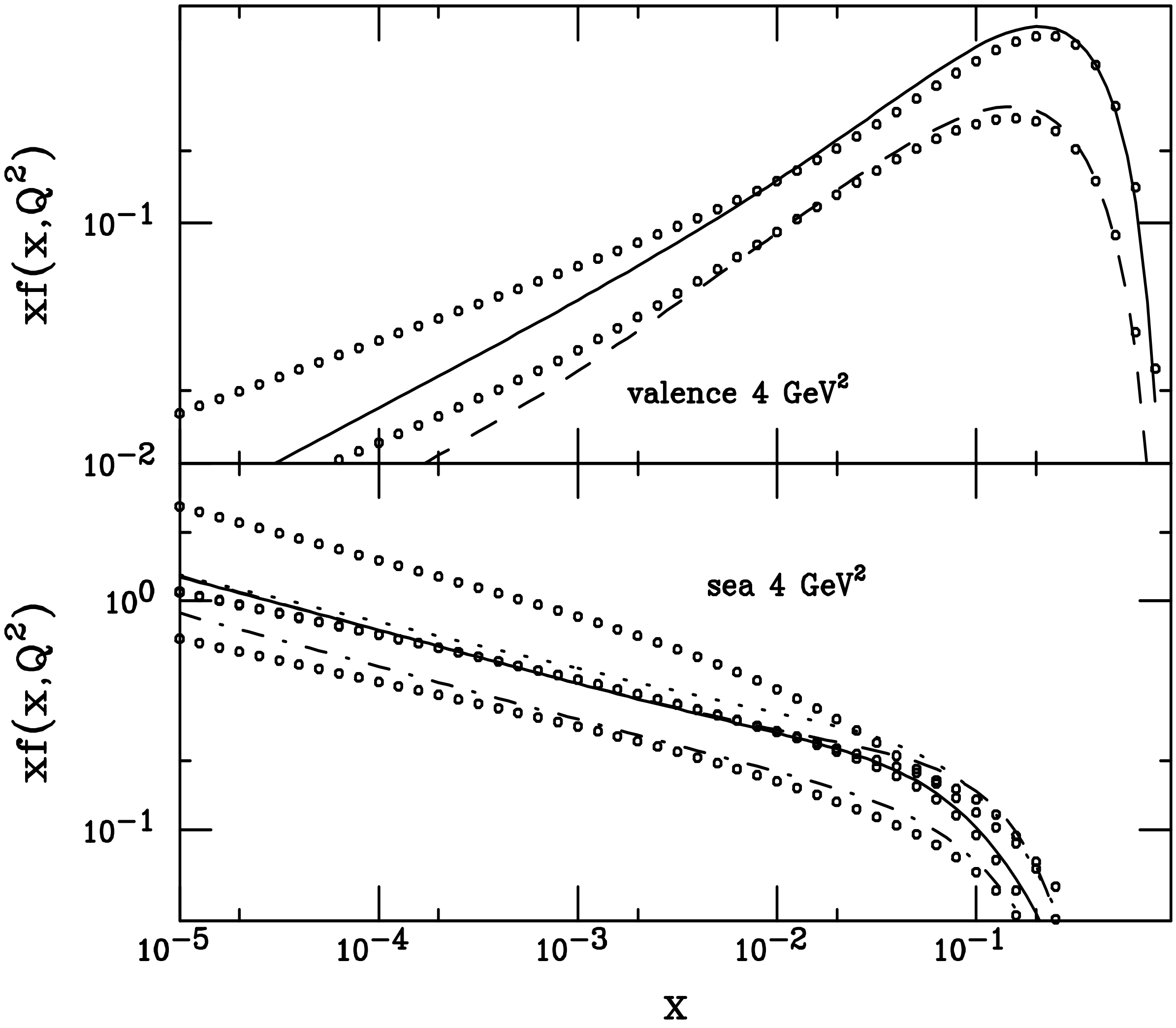

Figure 26: We compare the MRST HO and MRST LO central gluon sets of parton densities. The curves show the HO set while the points are for the LO set. The upper plot shows the up (solid) and down (dashed) valence quark densities. The lower plot shows the sea and gluon distributions for $\overline{u}$ (solid), $\overline{d}$ (dashed), $\overline{s}$ (dot-dashed), and $0.1g$ (dotted). The corresponding LO distributions are the curves with the points closest to the curves. All the results are shown for $Q^2 = 4\ \mathrm{GeV}^2$.

LO and NLO Parton Densities at $Q^2 = 100$ GeV^2

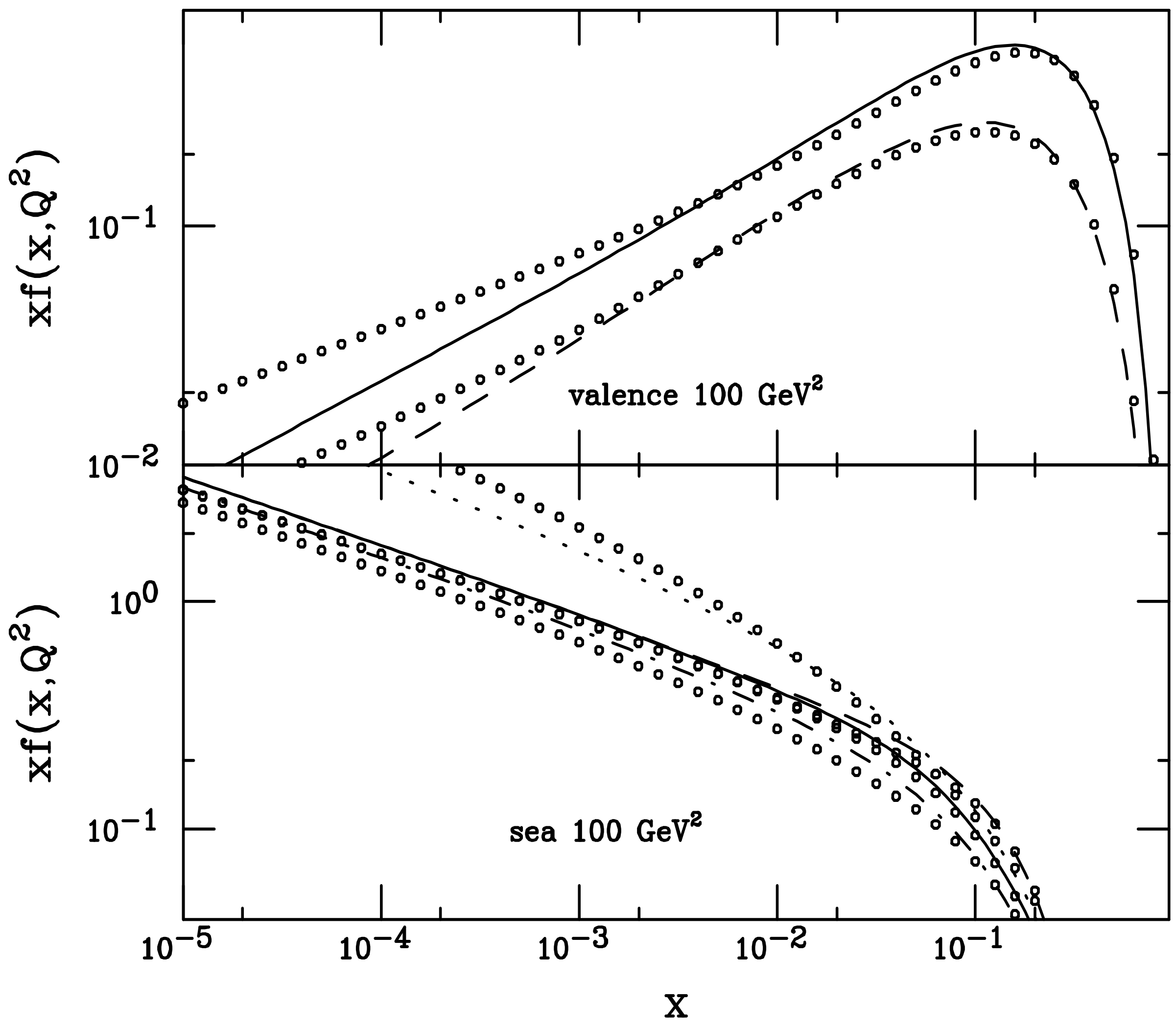

Figure 27: We compare the MRST HO and MRST LO central gluon sets of parton densities. The curves show the HO set while the points are for the LO set. The upper plot shows the up (solid) and down (dashed) valence quark densities. The lower plot shows the sea and gluon distributions for $\overline{u}$ (solid), $\overline{d}$ (dashed), $\overline{s}$ (dot-dashed), and $0.1g$ (dotted). The corresponding LO distributions are the curves with the points closest to the curves. All the results are shown for $Q^2 = 100$ GeV^2.

Comparison of Charm Cross Sections at LO and NLO

	$\sigma(c\overline{c})$ (μb)				
	MRST LO			MRST HO	
$\sqrt{s}$ (GeV)	$\sigma_{c\overline{c}}^{\mathrm{LO}(1)}$	$\sigma_{c\overline{c}}^{\mathrm{LO}(2)}$	$\sigma_{c\overline{c}}^{\mathrm{NLO}}$	$\sigma_{c\overline{c}}^{\mathrm{LO}(2)}$	$\sigma_{c\overline{c}}^{\mathrm{NLO}}$
17.3	1.95	1.56	4.16	1.85	5.54
19.4	2.70	2.16	5.65	2.67	7.87
29.1	7.37	5.84	14.52	8.04	22.36
38.8	13.55	10.60	25.85	15.10	40.57
63	33.29	25.37	60.74	35.79	91.88
200	188.5	132.6	314.1	152.8	381.7
500	573.3	374.9	897.0	356.8	922.8
5500	5772	3040	7733	2002	5833
14000	11760	5668	14920	3332	10240

Table 6: Total $c\overline{c}$ production cross sections at fixed-target and collider energies. The (1) or (2) superscript indicates whether α_s was calculated at one or two loops.

Comparison of Bottom Cross Sections at LO and NLO

	$\sigma(b\bar{b})$ (μb)				
	MRST LO			MRST HO	
$\sqrt{s}$ (GeV)	$\sigma_{b\bar{b}}^{\rm LO(1)}$	$\sigma_{b\bar{b}}^{\rm LO(2)}$	$\sigma_{b\bar{b}}^{\rm NLO}$	$\sigma_{b\bar{b}}^{\rm LO(2)}$	$\sigma_{b\bar{b}}^{\rm NLO}$
63	0.047	0.0374	0.0688	0.0394	0.0763
200	0.942	0.744	1.371	0.987	1.903
500	5.01	3.825	7.422	4.809	9.799
5500	122.0	82.71	186.3	72.85	186.3
14000	328.0	211.0	502.2	164.5	454.1

Table 7: Total $b\bar{b}$ production cross sections at collider energies. The (1) or (2) superscript indicates whether α_s was calculated at one or two loops.

LO and NLO Charm Distributions at RHIC

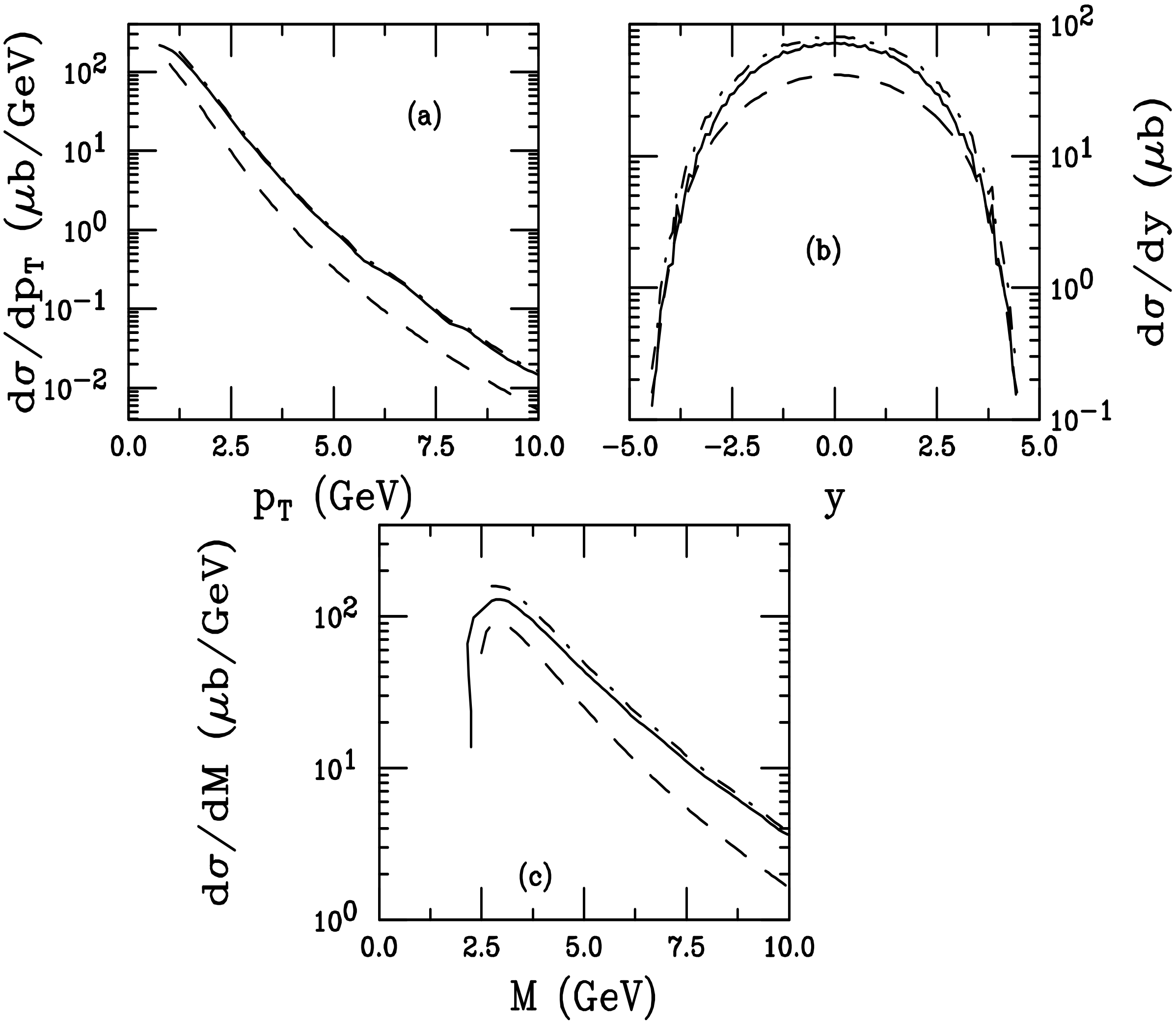

Figure 28: The charm quark p_T (a), rapidity (b), and $c\bar{c}$ pair mass (c) for a full NLO calculation (solid), a full LO calculation (dashed) and LO for $\mathcal{O}(\alpha_s^2)$ plus NLO for $\mathcal{O}(\alpha_s^3)$ (LO+NLO) (dot-dashed). The calculations are for pp collisions at 200 GeV, no nuclear effects included.

Charm K Factors at RHIC

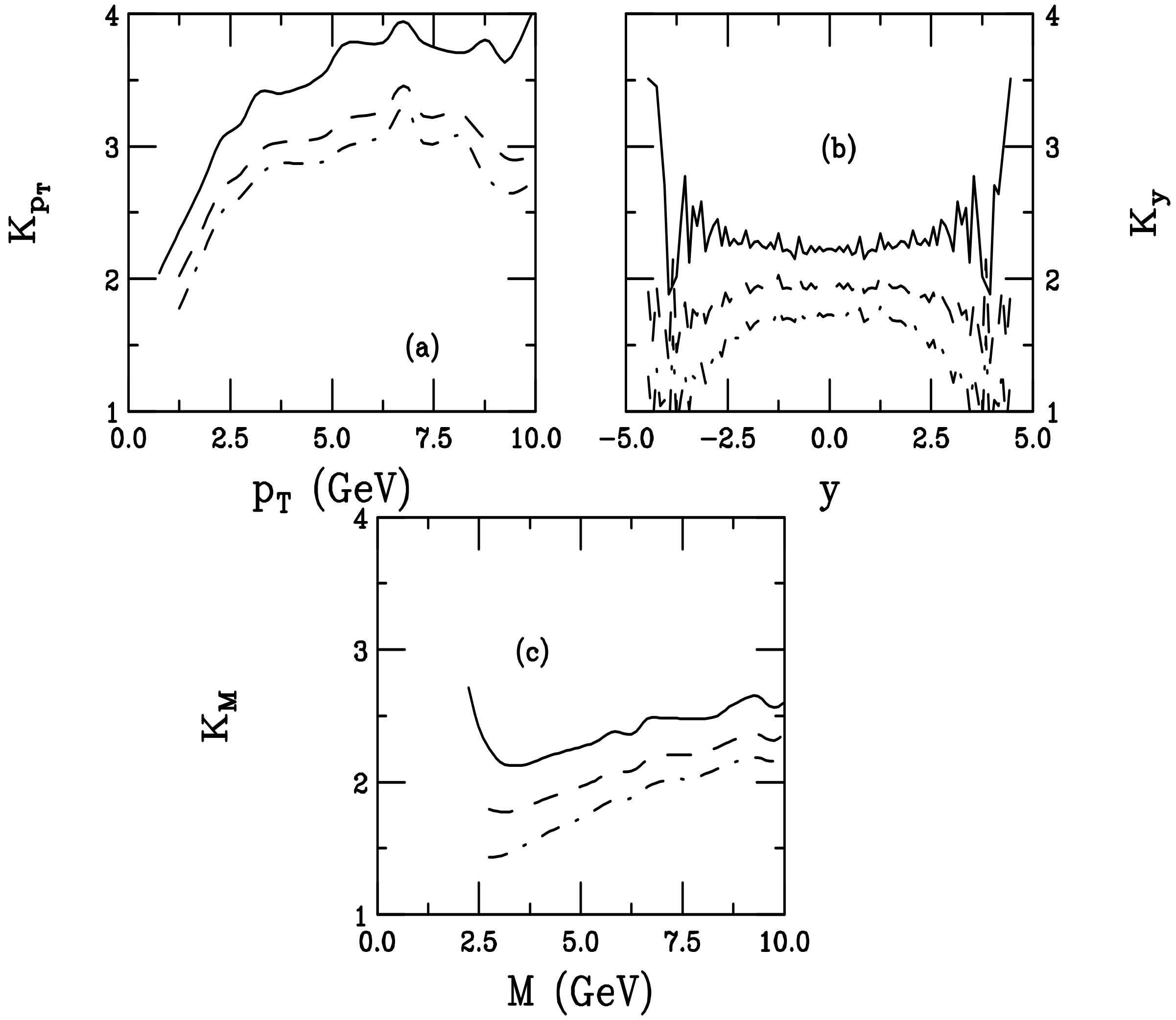

Figure 29: The K factors as a function of charm quark p_T (a), rapidity (b), and $c\bar{c}$ pair mass (c) for full NLO/LO with same parameters (solid), LO+NLO/full LO (dashed) and full NLO/full LO (dot-dashed).

LO and NLO Bottom Distributions at RHIC

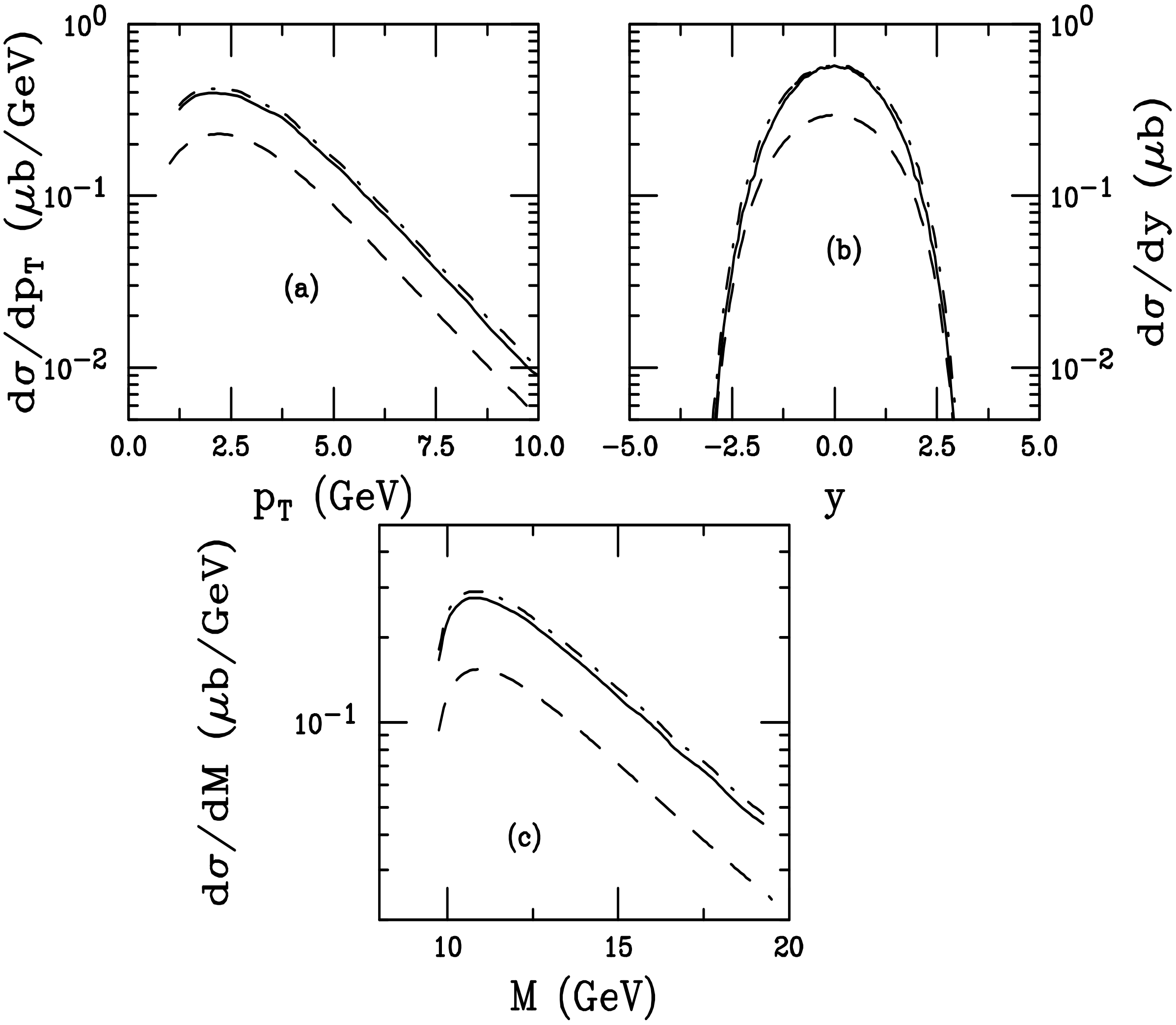

Figure 30: The bottom quark p_T (a), rapidity (b), and $b\overline{b}$ pair mass (c) for a full NLO calculation (solid), a full LO calculation (dashed) and LO for $\mathcal{O}(\alpha_s^2)$ plus NLO for $\mathcal{O}(\alpha_s^3)$ (LO+NLO) (dot-dashed). The calculations are for pp collisions at 200 GeV, no nuclear effects included.

Bottom K Factors at RHIC

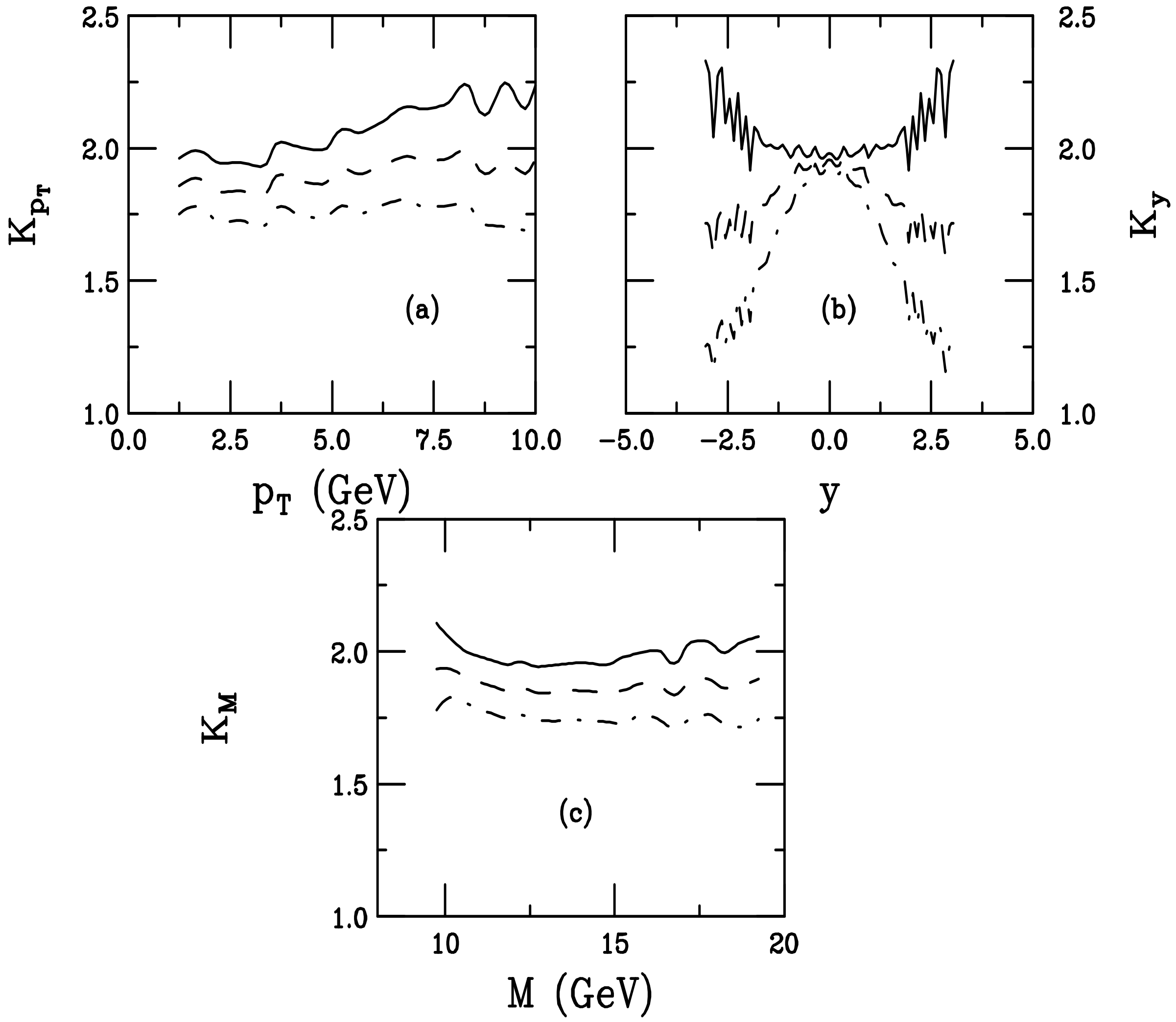

Figure 31: The K factors as a function of bottom quark p_T (a), rapidity (b), and $b\overline{b}$ pair mass (c) for full NLO/LO with same parameters (solid), LO+NLO/full LO (dashed) and full NLO/full LO (dot-dashed).

LO and NLO Charm Distributions at LHC

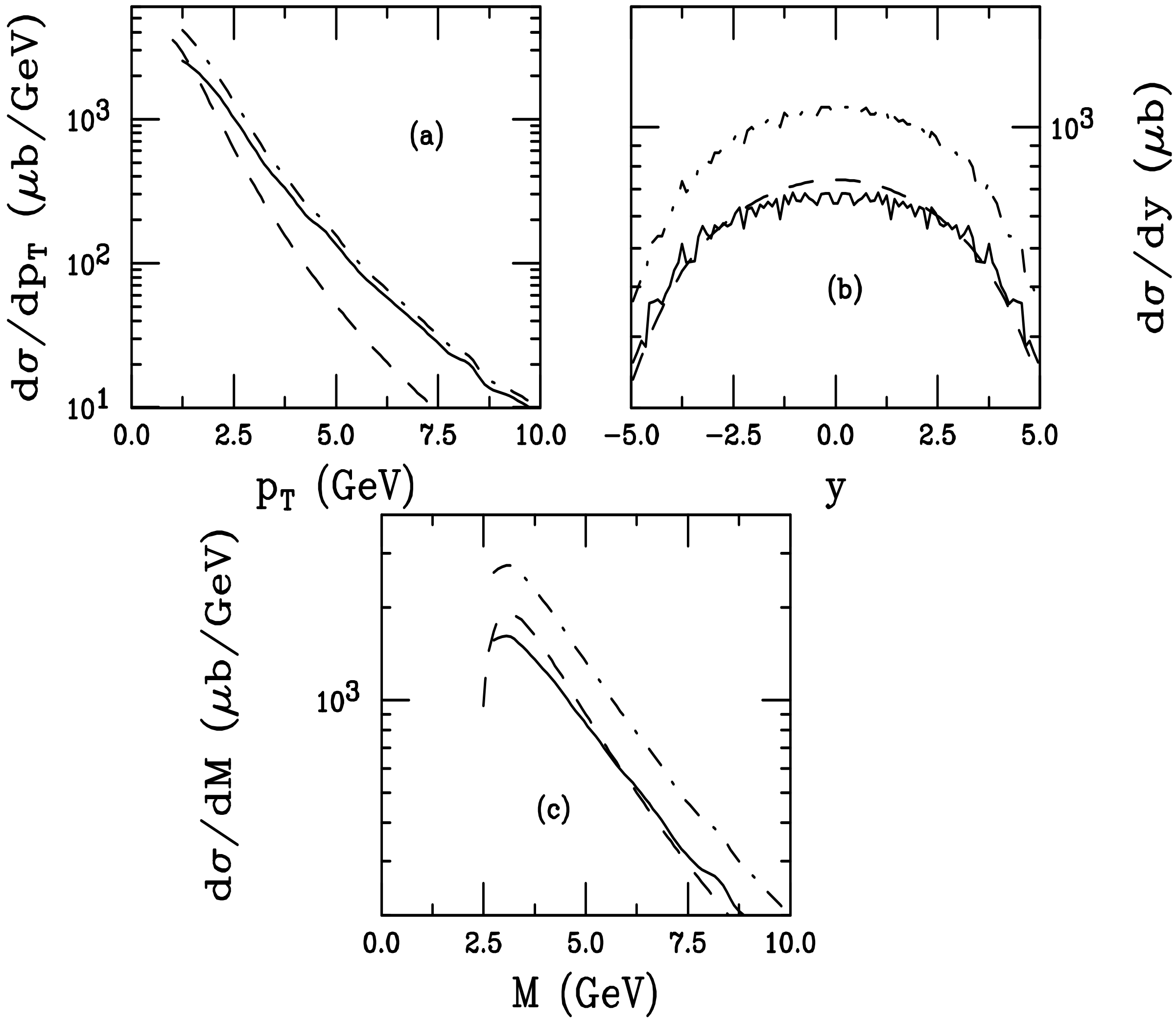

Figure 32: The charm quark p_T (a), rapidity (b), and $c\bar{c}$ pair mass (c) for a full NLO calculation (solid), a full LO calculation (dashed) and LO for $\mathcal{O}(\alpha_s^2)$ plus NLO for $\mathcal{O}(\alpha_s^3)$ (LO+NLO) (dot-dashed). The calculations are for pp collisions at 5.5 TeV, no nuclear effects included.

Charm K Factors at LHC

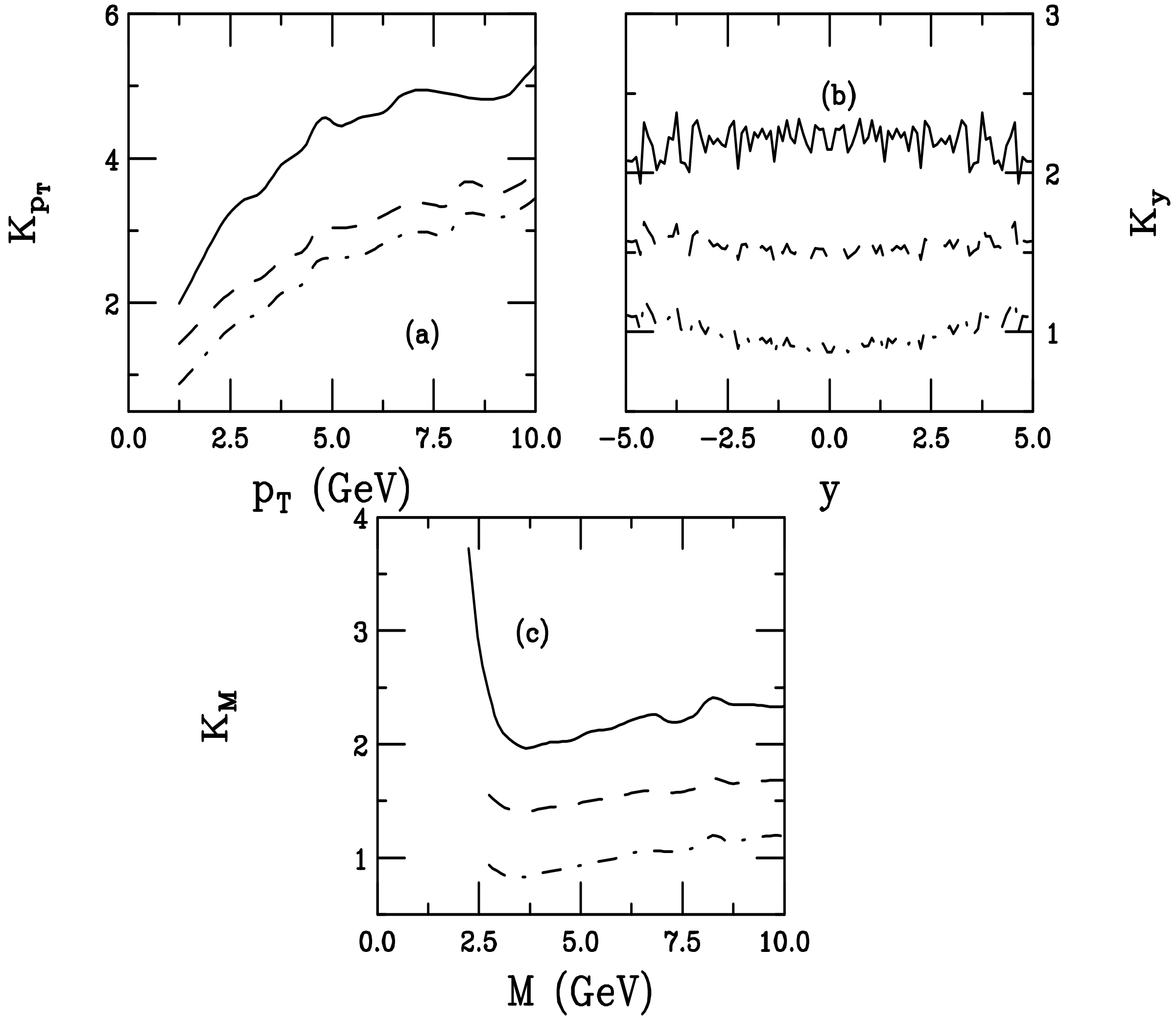

Figure 33: The K factors as a function of charm quark p_T (a), rapidity (b), and $c\bar{c}$ pair mass (c) for full NLO/LO with same parameters (solid), LO+NLO/full LO (dashed) and full NLO/full LO (dot-dashed).

LO and NLO Bottom Distributions at LHC

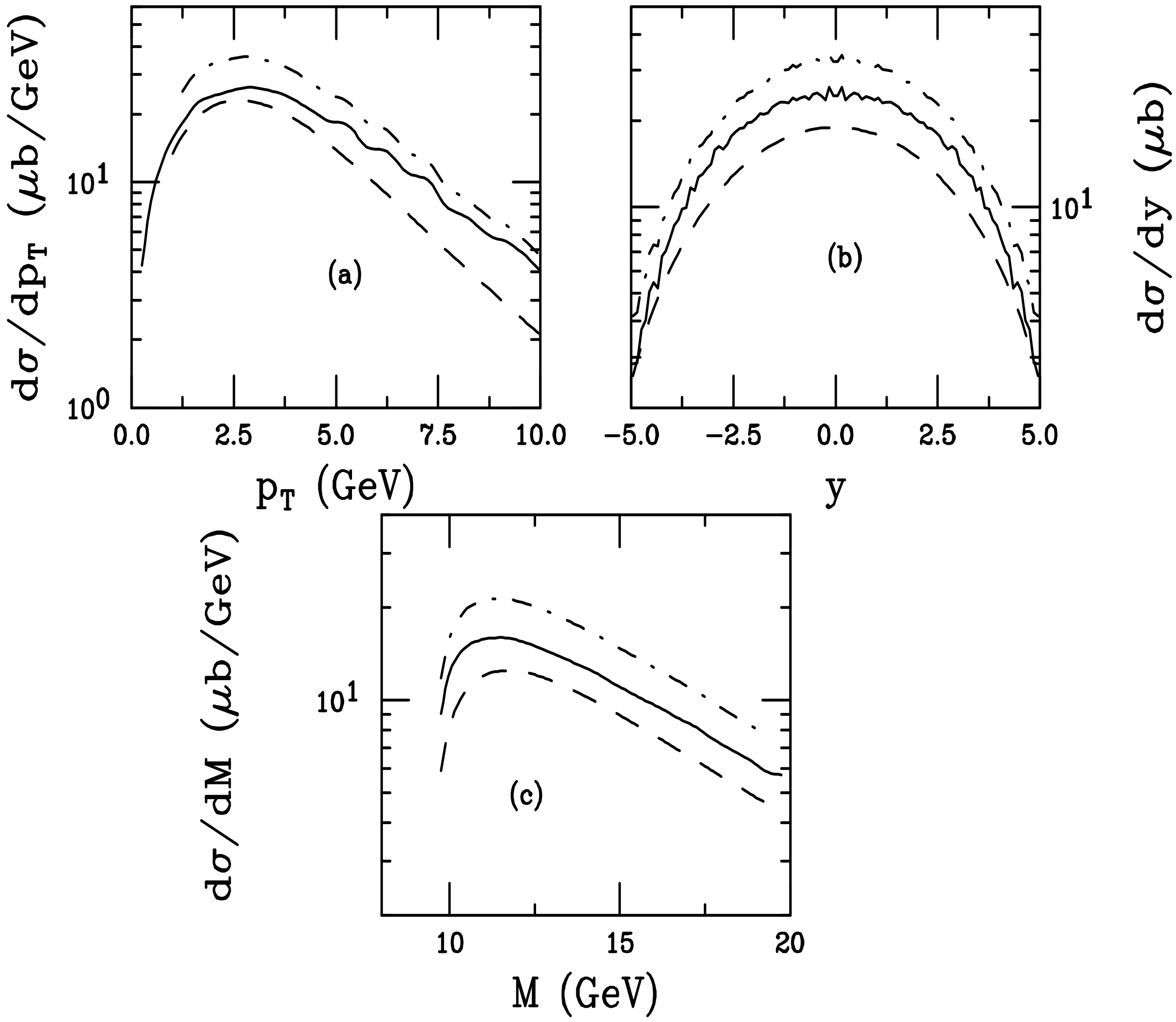

Figure 34: The bottom quark p_T (a), rapidity (b), and $b\bar{b}$ pair mass (c) for a full NLO calculation (solid), a full LO calculation (dashed) and LO for $\mathcal{O}(\alpha_s^2)$ plus NLO for $\mathcal{O}(\alpha_s^3)$ (LO+NLO) (dot-dashed). The calculations are for pp collisions at 5.5 TeV, no nuclear effects included.

Bottom K Factors at LHC

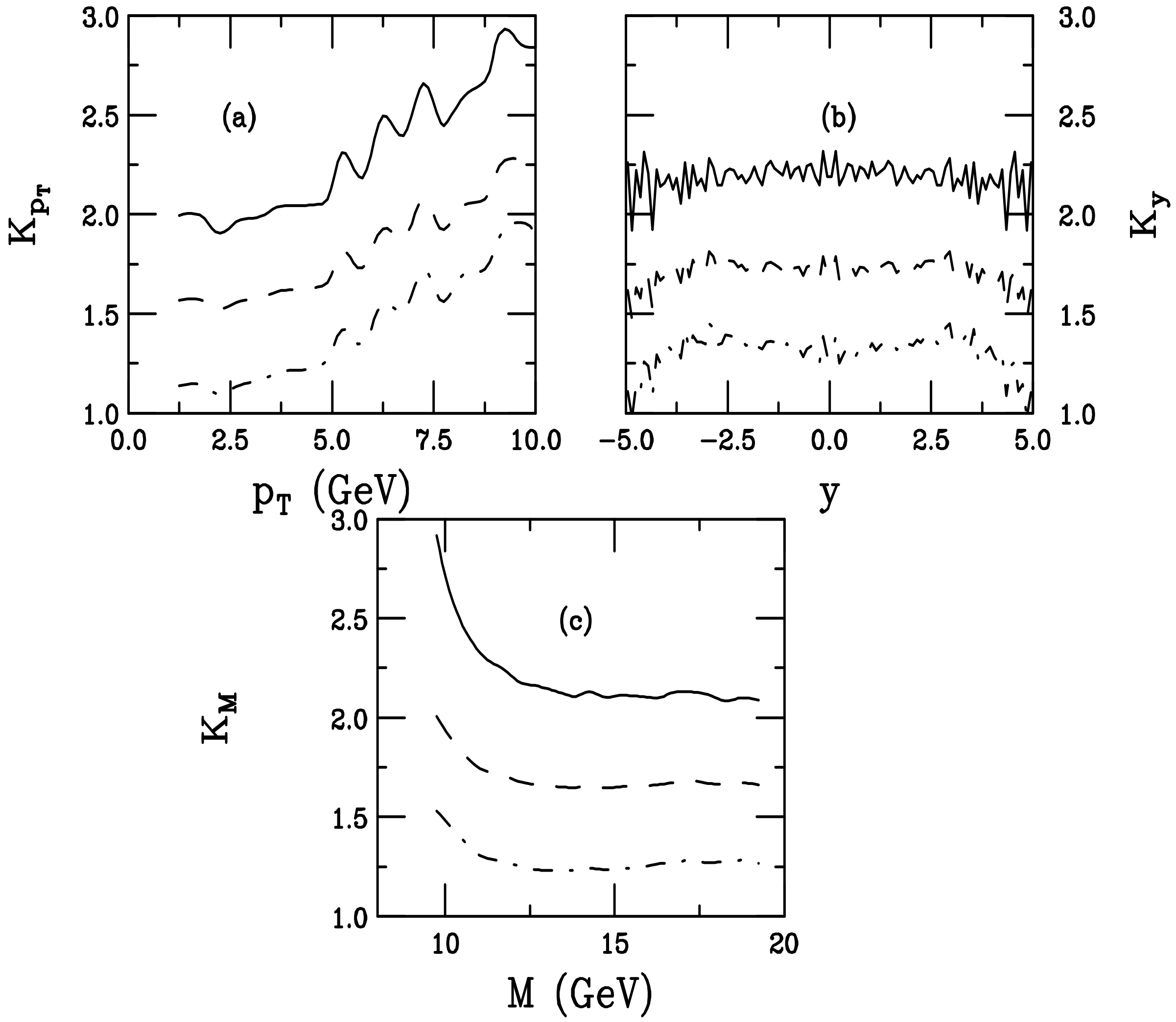

Figure 35: The K factors as a function of bottom quark p_T (a), rapidity (b), and $b\bar{b}$ pair mass (c) for full NLO/LO with same parameters (solid), LO+NLO/full LO (dashed) and full NLO/full LO (dot-dashed).

Conclusions

- New calculations of quarkonium rates at LHC using latest PDFs and updated Tevatron data
- Cross sections can vary by a factor of two depending on scenario
- Total rates high for J/ψ and Υ, high enough for precision measurements
- More reliable lattice studies of quarkonium potential suggests that suppression of some quarkonium states due to chiral symmetry restoration, *not* deconfinement
- Υ suppression should be most important deconfinement test
- Regeneration of J/ψ and Υ possible due to coalescence mechanisms
- Normalization of quarkonium yields to total $Q\overline{Q}$ important to look for possible enhancements